Rovibrational Energy Transfer in the $4\nu_{CH}$ Manifold of Acetylene, Viewed by IR−UV Double-Resonance Spectroscopy. 4. Collision-Induced Quasi-Continuous Background Effects†

Mark A. Payne, Angela P. Milce, Michael J. Frost,‡ and Brian J. Orr*

Centre for Lasers and Applications, Macquarie University, Sydney, NSW 2109, Australia

Received: September 16, 2005; In Final Form: January 12, 2006

The $4\nu_{CH}$ rovibrational manifold around 12 700 cm^{-1} in the electronic ground state, $\tilde{X}$, of acetylene (C_2H_2) is monitored by time-resolved infrared-ultraviolet double-resonance (IR−UV DR) spectroscopy. An IR laser pulse initially prepares rotational J states, associated with the "IR-bright" ($\nu_1 + 3\nu_3$) or $(1\ 0\ 3\ 0\ 0)^0$ vibrational combination level, and subsequent collision-induced state-to-state energy transfer is probed by UV laser-induced fluorescence. Anharmonic, l-resonance, and Coriolis couplings affect the J states of interest, resulting in a congested rovibrational manifold that exhibits complex intramolecular dynamics. In preceding papers in this series, we have described three complementary forms of the IR−UV DR experiment (IR-scanned, UV-scanned, and kinetic) on collision-induced rovibrational satellites, comprising both regular even-ΔJ features and unexpected odd-ΔJ features. This paper examines an unusual collision-induced quasi-continuous background (CIQCB) effect that is apparently ubiquitous, accompanying regular even-ΔJ rovibrational energy transfer and accounting for much of the observed collision-induced odd-ΔJ satellite structure; certain IR-bright $(1\ 0\ 3\ 0\ 0)^0$ rovibrational states (e.g., $J = 12$) are particularly prominent in this regard. We examine the mechanism of this CIQCB phenomenon in terms of a congested IR-dark rovibrational manifold that is populated by collisional transfer from the nearly isoenergetic IR-bright $(1\ 0\ 3\ 0\ 0)^0$ submanifold.

I. Introduction

Time-resolved optical double-resonance (DR) spectroscopy, using successive laser pulses for pumping and probing, is a well-established way to explore the energetics, energy-transfer dynamics, and reactivity of polyatomic molecules. In particular, collision-induced state-to-state energy transfer in the gas phase is of long-standing intrinsic interest,[1−7] with ongoing challenges presented by highly excited rovibrational manifolds (e.g., above ∼10 000 cm^{-1}) of small polyatomic molecules with just a few atoms (e.g., 3−6). Such rovibrational manifolds are congested and relevant in other contexts such as chemical reaction dynamics[7−14] and intramolecular vibrational redistribution (IVR).[10,15−17] Moreover, intramolecular perturbations influence collision-induced energy-transfer efficiencies in small polyatomics,[4−6] contrasting with the more highly congested rovibrational manifolds in larger polyatomic molecules.

An especially advantageous form of time-resolved DR spectroscopy comprises a rovibrational pumping and rovibronic probing sequence. Rovibronic transition probabilities associated with probe excitation can then effectively project out distinctive aspects of the rovibrational manifold in which pumping takes place, thereby supplementing spectroscopic information that is directly accessible by simple rovibrational absorption spectroscopy alone. The timing of the optical DR excitation sequence on nanosecond (ns) time scales can then be used to characterize state-resolved molecular dynamical processes. Such an approach is most informative in the case of highly excited small polyatomic molecules, such as acetylene (C_2H_2)[18−32] and NO_2,[33,34] where individual rovibrational J states can be pumped and probed state-selectively to investigate the related dynamical processes.

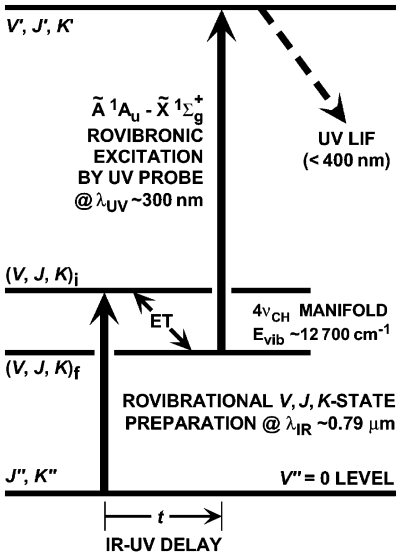

Figure 1. Excitation scheme for time-resolved, LIF-detected IR−UV DR spectroscopy of C_2H_2. Discrete rovibrational states $(V, J, K)_i$ and $(V, J, K)_f$ in the $4\nu_{CH}$ manifold at ∼12 700 cm^{-1} are coupled by collision-induced energy transfer (ET) during the IR−UV delay interval, t.

In this paper, we use pulsed tunable infrared (IR) and ultraviolet (UV) lasers for time-resolved DR spectroscopy to investigate the $4\nu_{CH}$ rovibrational manifold at ∼12 700 cm^{-1} in the $\tilde{X}^1\Sigma_g^+$ electronic ground state of C_2H_2. A similar IR−UV DR approach has been used in the previous three papers of this series,[30−32] preceded by our earlier IR−UV DR experiments of the same manifold[28,29] and of the 11 600 cm^{-1} ($\nu_{CC} + 3\nu_{CH}$) manifold.[24−27] Much of our general methodology emulates the previous work of Crim and co-workers, who identified the key role of IR-dark/UV-bright channels and vice versa.[19−23]

Figure 1 depicts our time-resolved IR−UV DR spectroscopic excitation scheme for C_2H_2, with a $4\nu_{CH}$ band transition $(V, J, K)_i \leftarrow (V'' = 0, J'', K'')$ selectively excited by a narrowband

† Part of the special issue "Jürgen Troe Festschrift".

* To whom correspondence should be addressed. E-mail: brian.orr@mq.edu.au.

‡ Present address: School of Engineering and Physical Sciences, Heriot-Watt University, Riccarton, Edinburgh, EH14 4AS, U.K. E-mail: M.J.Frost@hw.ac.uk.

10.1021/jp055245i CCC: $33.50
Published on Web 02/04/2006

tunable IR PUMP laser pulse. A double-headed arrow represents energy transfer (ET) within the $4\nu_{CH}$ manifold, from the prepared rovibrational state $(V, J, K)_i$ to a destination rovibrational state $(V, J, K)_f$. Under the conditions of our IR−UV DR experiments in gas-phase C_2H_2 at pressure P, this ET is induced by collisions during a controllable IR−UV delay interval, t. A tunable UV PROBE laser pulse is then used to excite rovibronic transitions $(V', J', K') \leftarrow (V, J, K)_f$ in the $\tilde{A}-\tilde{X}$ absorption system, detected by laser-induced fluorescence (LIF) from the $\tilde{A}\ ^1A_u$ electronic manifold. These ET processes depend on the combination of IR−UV delay, t, and sample pressure, P, defining the collision number, z, which, as before,[24−32] is referred to Lennard−Jones collisional rate constants, k_{LJ}. (Values of z, for C_2H_2/C_2H_2 self-collisions at 300 K,[22] are referred to $k_{LJ} = 16.4\ \mu s^{-1}\ Torr^{-1} = 5.10 \times 10^{-10}\ cm^3\ molecule^{-1}\ s^{-1}$.)

Of central interest in the context of Figure 1 are collision-induced state-to-state ET processes between discrete rovibrational states $(V, J, K)_i$ and $(V, J, K)_f$ within the C_2H_2 $4\nu_{CH}$ manifold. These include both pure rotational ET (RET), within a single vibrational level (i.e., $V_i \equiv V_f$), and vibration-to-vibration (V−V) ET, which is vibrationally inelastic (i.e., $V_i \neq V_f$). Effectively collision-free conditions, with $t \approx 0$ and/or $z \approx 0$, result in direct excitation where $(V, J, K)_i \equiv (V, J, K)_f$; IR−UV DR spectra (either IR- or UV-scanned) then comprise a set of characteristic "parent" peaks. As t and z are increased, the parent peaks in IR−UV DR spectra become less prominent and give way to a variety of satellite peaks arising from collision-induced ET processes. Apart from IR-scanned IR−UV DR spectra (with fixed UV wavelength and z) and UV-scanned IR−UV DR spectra (with fixed IR wavelength and z), it is also informative to record IR−UV DR kinetics by scanning t (and hence z, at a set value of P) with IR and UV wavelengths fixed on discrete features in the IR−UV DR spectra. As in previous work,[24−32] our experiments rely vitally on these three complementary approaches.

A substantial body of knowledge on the spectroscopy and structure of C_2H_2 has been reviewed in earlier papers of this series,[30−32] with emphasis on high-energy vibrational levels above $\sim$10 000 cm^{-1} in the $\tilde{X}\ \Sigma_g^{1+}$ electronic ground state. Most of these levels can be grouped in polyads or clusters, defined by dynamically relevant constants of motion, and are influenced by a variety of intramolecular perturbations due to anharmonic mixing, l-resonance effects, and Coriolis coupling. It suffices here to note that an extensive spectroscopic database is available[35−39] to sustain ongoing interest in the congested, strongly perturbed nature of such levels. It should also be recognized that the 11 600 cm^{-1} ($\nu_{CC} + 3\nu_{CH}$) region[24−27] and the 12 700 cm^{-1} $4\nu_{CH}$ region,[28−32] on which our IR−UV DR investigations have focused, correspond to excitation energies that are relatively high but nevertheless not high enough to be considered "chemically significant". For instance, they are well below the threshold (above 15 000 cm^{-1}) for isomerization of C_2H_2 to vinylidene ($H_2C{=}C{:}$), which is of much mechanistic interest.[40−47]

This paper addresses unusual J-resolved dynamical behavior in the $4\nu_{CH}$ manifold, apparently associated with a collision-induced quasi-continuous background (CIQCB).[29−32] A postulated form of this phenomenon is portrayed schematically in Figure 2. In contrast to Figure 1, collision-induced ET is understood to populate a bath of destination states $(V, J, K)_f$ that are IR-dark but UV-bright and yield diffuse LIF-detected UV PROBE excitation to rovibronic levels (V', J', K') but not necessarily terminating in the $\tilde{A}\ ^1A_u$ manifold of C_2H_2. Figure 2 depicts a quasi-continuous rovibrational manifold that gives

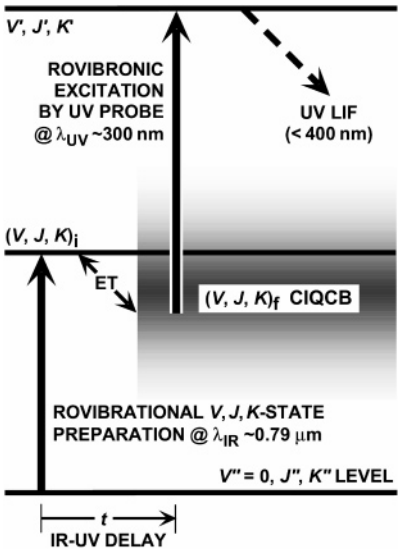

Figure 2. Excitation scheme depicting the postulated collision-induced quasi-continuous background (CIQCB, represented by a shaded region) that is detected by time-resolved, LIF-detected IR−UV DR spectroscopy in the $\sim$12 700 cm^{-1} $4\nu_{CH}$ rovibrational manifold of C_2H_2. As in Figure 1, the IR PUMP prepares a discrete rovibrational state $(V, J, K)_i$. However, subsequent collision-induced rovibrational energy transfer (ET) evidently leads instead to a quasi-continuous manifold of background states $(V, J, K)_f$ that can be detected uniformly as a CIQCB over a wide range of UV PROBE wavelengths.

rise to collision-induced IR−UV DR signals over a wide range of UV PROBE wavelengths, even when they do not coincide with discrete transitions in rovibronic LIF-excitation spectra from IR-bright levels. Such CIQCB effects are unexpected at rovibrational excitation energies as low as $\sim$12 700 cm^{-1}. Moreover, they are associated with a number of apparent anomalies, such as unexpected (nominally forbidden) odd-ΔJ RET and/or V−V ET, that are observed in the $4\nu_{CH}$ region of C_2H_2.

Our IR−UV DR kinetic results can be modeled satisfactorily in a manner consistent with Figure 2.[49,50] Nevertheless, another possible CIQCB model, to be considered in Section IV of this paper, comprises a discrete submanifold of IR-dark destination states $(V, J, K)_f$ that are viewed by UV PROBE transitions to a quasi-continuous distribution of rovibronically excited states from which LIF is observed.

Here we address these unusual CIQCB effects more comprehensively than in our previous papers.[29−32] We examine IR−UV DR spectra pumped in the $4\nu_{CH}$ region of the IR absorption spectrum, which derives oscillator strength from an "IR-bright" $\Sigma_u^+ - \Sigma_g^+$ rovibrational combination band centered at 12 675.68 cm^{-1} with zero-order label ($\nu_1 + 3\nu_3$).[48] Here, ν_1 (σ_g^+) and ν_3 (σ_u^+) denote the two CH stretching normal modes; the upper and lower vibrational levels of this band have zero-order labels $(1\ 0\ 3\ 0\ 0)^0$ and $(0\ 0\ 0\ 0\ 0)^0$, respectively, in terms of basis states $(V_1\ V_2\ V_3\ V_4\ V_5)^l$, where V_i designates vibrational quanta in each of the five normal modes ($i = 1-5$) and l is the resultant vibrational angular momentum.

In Section II, we present IR−UV DR spectra probed by LIF excitation at 322−326 nm in the vicinity of the $\tilde{A}-\tilde{X}\ 1_1^0\ 3_3^0\ (4_0\ 6_0)^1$ rovibronic band.[31] Section III contains corresponding IR−UV DR results with C_2H_2 probed via the $\tilde{A}-\tilde{X}\ 1_1^0\ 3_3^1\ 5_0^1$ rovibronic band at $\sim$299 nm.[30,31] CIQCB effects are evident in each of these Sections. Section IV addresses significant mechanistic questions with regard to the CIQCB, while concluding remarks appear in Section V. Details of a kinetic master-

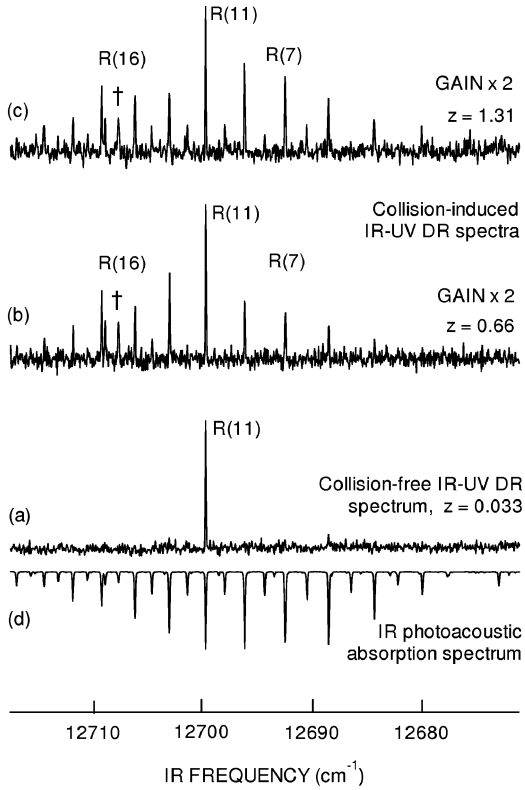

Figure 3. IR PUMP-scanned, LIF-detected IR−UV DR spectra (a−c) in the 12 676 cm^{-1} ($\nu_1 + 3\nu_3$) band of C_2H_2 ($P = 0.20$ Torr, $T = 300$ K) with the UV PROBE wavelength set at 323.791 nm to monitor the $(1\ 0\ 3\ 0\ 0)^0$ $J_f = 12$ rovibrational state. IR−UV delay times, t, and Lennard−Jones collision numbers, z, are varied as follows: (a) $t = 10$ ns, $z = 0.033$; (b) $t = 200$ ns, $z = 0.66$; (c) $t = 400$ ns, $z = 1.31$. Trace d is a photoacoustic absorption spectrum, recorded with C_2H_2 pressure $P = 30$ Torr.

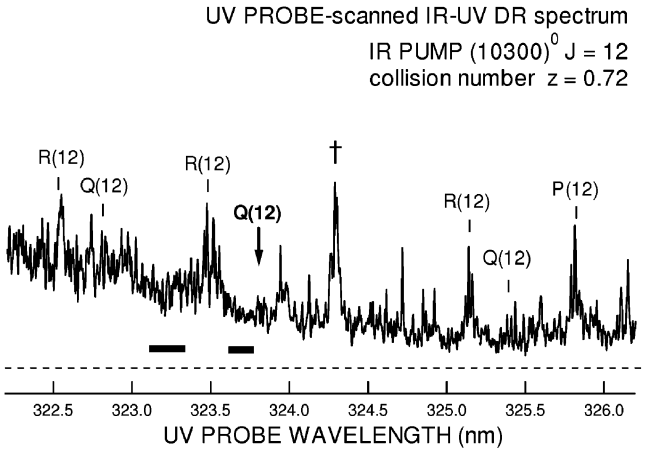

Figure 4. Collision-induced UV-scanned IR−UV DR spectra of C_2H_2 ($P = 0.22$ Torr, $T = 300$ K, $t = 200$ ns, $z = 0.72$), recorded with the IR PUMP preparing molecules in the $(1\ 0\ 3\ 0\ 0)^0$ $J_i = 12$ rovibrational state and the UV PROBE wavelength scanned in the vicinity of the $\tilde{A}-\tilde{X}$ $1_1^0\,3_3^0\,(4_0\,6_0)^1$ rovibronic absorption band at ~322−326 nm. The dashed horizontal line shows the level of scattered light detected when the IR PUMP beam is blocked. Clearly separated from the dashed line is a quasi-continuous background of IR−UV DR signal amplitude, as well as discrete IR−UV DR parent and RET satellites projected out of the background signal. See the text for further details of this CIQCB effect.

equation model[31,32,49] that accommodates CIQCB effects and related J-specific ET gateways will be reported elsewhere.[50]

II. IR−UV DR Spectra with UV Probe at ~324 nm

With an IR−UV DR excitation scheme as in Figure 1 and instrumentation as described previously,[30] ($\nu_1 + 3\nu_3$)-band spectra of C_2H_2 are presented in Figure 3 (which is an extended version of Figure 1 in ref 31). Traces a−c are IR-scanned IR−UV DR spectra of C_2H_2 gas ($P = 0.20$ Torr, $T = 300$ K), accompanied in trace d by a corresponding photoacoustic absorption reference spectrum. The IR PUMP radiation, at ~790 nm with optical bandwidth ~0.08 cm^{-1} and pulse duration ~7 ns, is generated by Raman-shifting output from a Nd:YAG-pumped tunable dye laser system.[30] The UV PROBE wavelength is set at 323.791 nm, which corresponds in the IR−UV DR excitation scheme to an intermediate rovibrational state $(V, J, K)_f$ that is identified as $(1\ 0\ 3\ 0\ 0)^0$ $J_f = 12$;[31] this state has been proposed[29−32,49,50] as a primary gateway for odd-ΔJ collision-induced ET in the $4\nu_{CH}$ manifold of C_2H_2. The effectively collision-free IR−UV DR spectrum in trace a, with $z \approx 0$, comprises the directly excited R(11) peak with $(V, J, K)_i \equiv (V, J, K)_f$, plus a single P(13) peak beyond the limit of Figure 3. (These two $J = 12$ parent peaks are known[48] to occur at 12 699.96 cm^{-1} and 12 641.15 cm^{-1}, respectively.)

The other two IR−UV DR spectra in Figure 3 were recorded with (b) 20- and (c) 40-fold increases in IR−UV delay, t (and hence z, with fixed $P = 0.20$ Torr), and twice the instrumental gain of trace a. They comprise prominent collision-induced R(J − 1) features, with even values of J (= 2−10 and 14−22), that is, customary even-ΔJ collision-induced RET satellites as expected for a centrosymmetric linear molecule such as C_2H_2. There are also unexpected odd-ΔJ collision-induced RET satellites, R(J − 1) with odd values of J (= 7−21); the prominence of the R(16) feature, marked by a dagger in Figure 3b and c, suggests the $(1\ 0\ 3\ 0\ 0)^0$ $J = 17$ state as a secondary gateway for apparent odd-ΔJ collision-induced ET. A tiny R(5) feature in trace a indicates that the $(1\ 0\ 3\ 0\ 0)^0$ $J = 6$ rovibrational state may also be monitored weakly at this UV PROBE wavelength; however, this too is an even-J state and so its RET is not expected to contaminate the odd-ΔJ satellite structure pertaining to the probed $(1\ 0\ 3\ 0\ 0)^0$ $J_f = 12$ state.

Odd-ΔJ IR−UV DR satellites as in Figure 3 were originally taken[28] to imply some form of collision-induced *a*/*s* nuclear-spin symmetry breaking, entailing (usually forbidden) interconversion of ortho and para nuclear-spin modifications of C_2H_2. These odd-ΔJ features were subsequently reinterpreted more plausibly[27,29−32] in terms of intramolecular rovibrational perturbations that spoil the vibrational angular momentum, l, and enable access to both e and f levels of l doublets[51] at a particular value of J.

It is significant that the R(11) IR−UV DR parent features in Figure 3b and c have almost identical amplitudes, rather than decaying as might be expected when t and z are increased twofold. It appears that, at the UV PROBE wavelength used here, the population of the $(1\ 0\ 3\ 0\ 0)^0$ $J_f = 12$ rovibrational state is replenished from another source other than direct IR PUMP excitation. We shall show in this paper that such effects are attributable to collision-induced ET from an IR-dark/UV-bright rovibrational manifold with a quasi-continuous UV PROBE spectrum, for example, as depicted tentatively in Figure 2.

CIQCB effects, on which this paper focuses, were first observed in the UV-scanned IR−UV DR spectrum shown in Figure 4. This is a survey spectrum (relatively rapidly scanned over a wide spectral range, with moderate signal-to-noise ratio) in which the IR PUMP frequency is set to coincide with the ($\nu_1 + 3\nu_3$)-band R(11) peak at 12 699.96 cm^{-1} that was

prominent in Figure 3a; this prepares C_2H_2 in an initial rovibrational state (V, J, K)$_i$ with label (1 0 3 0 0)^0 $J_i = 12$. With a large collision number, $z = 0.72$ (corresponding to $P = 0.22$ Torr and $t = 200$ ns at 300 K), the UV PROBE wavelength is scanned in the range of ~322−326 nm. This spans the $\tilde{A}-\tilde{X}$ $1_1^0\,3_3^0$ $(4_0\,6_0)^1$ rovibronic absorption band,[31] where ν_4' (a_u) and ν_6' (b_u) are Coriolis-coupled torsion and in-plane-bending modes in the $\tilde{A}$ ^1A_u manifold of C_2H_2, respectively.[52] The UV PROBE radiation, with optical bandwidth ~0.28 cm^{-1} and pulse duration ~15 ns, was generated as frequency-doubled output of an excimer-pumped tunable dye laser.[30] The spectrum shows much discrete (but poorly resolved, in view of the rapid scan rate) rovibronic structure. A few directly excited parent peaks are marked, including a Q(12) rovibronic feature designated by a boldface arrow at 323.791 nm, used as the fixed UV PROBE wavelength when Figure 3a−c was recorded. The parent peaks are accompanied by assorted collision-induced RET satellites, as expected at $z = 0.72$. (A corresponding collision-free, low-z spectrum was presented in Figure 4 of ref 31.) The central group of RET satellites, marked by a dagger at ~324.3 nm, is assigned to R-branch rovibronic transitions from even-J states of the (1 0 3 0 0)^0 submanifold, consistent with Figure 3b and c.

The dashed horizontal line in Figure 4 shows the level of scattered UV PROBE light (e.g., from the Brewster-angle windows, baffles, and walls of the cylindrical gas cell) detected by the LIF-sensing photomultiplier in the absence of the IR PUMP laser pulse (or with the IR PUMP tuned away from any IR absorption). A quasi-continuous background of IR−UV DR signal amplitude can be seen to separate unstructured portions of the IR−UV DR spectrum in Figure 4 from this scattered light level. The quasi-continuum extends across the entire UV-scanned region (~322−326 nm), with its amplitude diminishing twofold toward longer UV PROBE wavelength. Moreover, this background signal appears to be collision-induced, growing in as IR−UV delay, t, and collision number, z, increase.

It is remarkable that the CIQCB signal persists even where there are no discrete rovibronic features (as in two regions, each >0.1 nm wide, marked by horizontal bars in Figure 4). That is, the IR−UV DR signal level stays above the scattered light level even when the UV PROBE wavelength is off-resonance from any $\tilde{A}-\tilde{X}$ transitions originating from J states of the (1 0 3 0 0)^0 submanifold. It appears that the UV PROBE is able to excite LIF via $\tilde{A}-\tilde{X}$ transitions wherever it is scanned in these regions. Simple tests show that observation of the CIQCB signal requires both IR PUMP and UV PROBE laser pulses and that its amplitude cannot be attributed to any irregularities or to the power spectrum of the UV PROBE laser. As depicted schematically in Figure 2, we infer that the LIF-detected UV PROBE transitions that give rise to the CIQCB must originate from background states (V, J, K)$_f$ other than the well-characterized discrete states of the IR-bright (1 0 3 0 0)^0 submanifold. Evidence of CIQCB effects in IR-scanned IR−UV DR spectra such as Figure 3 are discernible via the odd-ΔJ ET satellites. Moreover, CIQCB effects are found[49] to persist when IR-scanned IR−UV DR spectra were recorded in the same 323-nm region by means of an advanced nonlinear-optical UV light source operating with a much narrower UV PROBE optical bandwidth (~0.06 cm^{-1}) over limited spectral ranges of ~3 cm^{-1}.[53]

III. IR−UV DR Spectra and Kinetics with UV PROBE at ~299 nm

As reported previously,[29] a more systematic study of CIQCB effects has been performed by probing the $\tilde{A}-\tilde{X}$ $1_1^0\,3_3^1\,5_0^1$ rovibronic band at ~299 nm,[28−31] where ν_3' (a_g) is an in-plane-bending mode and ν_5' (b_u) the CH stretching mode in the $\tilde{A}$ ^1A_u electronically excited manifold of C_2H_2. Here we review those results and expand on them to seek a better understanding of the dynamical processes involved. Figure 5 (adapted from Figure 4 in ref 29) shows UV-scanned IR−UV DR spectra, recorded in C_2H_2 gas ($P = 0.20$ Torr, $T = 300$ K) with the IR PUMP tuned to the ($\nu_1 + 3\nu_3$)-band R(11) peak, as in Figure 3a−c, thereby preparing the (1 0 3 0 0)^0 $J_i = 12$ state.

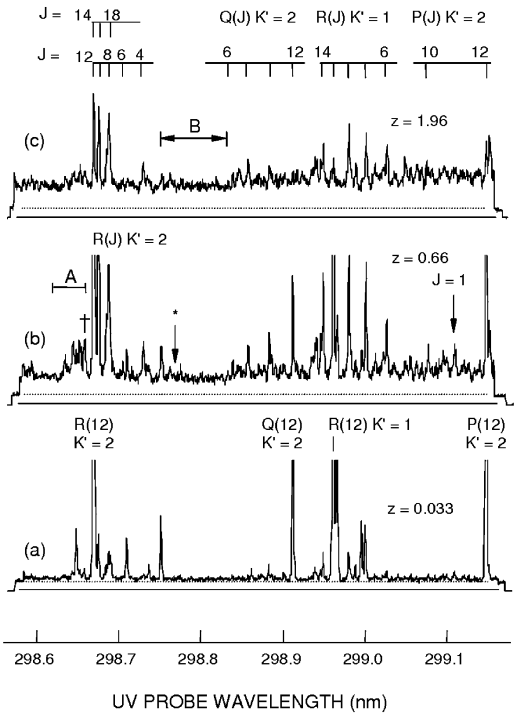

Figure 5. UV-scanned IR−UV DR spectra of C_2H_2 ($P = 0.20$ Torr, $T = 300$ K), recorded with the IR PUMP preparing molecules in the (1 0 3 0 0)^0 $J_i = 12$ rovibrational state and the UV PROBE wavelength scanned in the $\tilde{A}-\tilde{X}$ $1_1^0\,3_3^1\,5_0^1$ rovibronic band at ~299 nm.[29] The IR−UV delay, t, and Lennard−Jones collision number, z, are varied as follows: (a) $t = 10$ ns, $z = 0.033$; (b) $t = 200$ ns, $z = 0.66$; (c) $t = 600$ ns, $z = 1.96$. The dashed and solid horizontal lines show the levels of scattered (IR PUMP beam blocked) and "zero" (UV PROBE beam blocked) light, respectively. A collision-induced quasi-continuous background (CIQCB) of IR−UV DR signal amplitude grows in as z increases, underlying discrete IR−UV DR parent and RET satellites. See the text for further details.

In Figure 5, the UV PROBE (with optical bandwidth ~0.22 cm^{-1} and pulse duration ~15 ns) is scanned through the 299-nm $\tilde{A}-\tilde{X}$ $1_1^0\,3_3^1\,5_0^1$ rovibronic band. The resulting UV-scanned IR−UV DR spectra are recorded with instrumental gain an order of magnitude higher than is customary (e.g., as in Figure 3a−c), such that the (1 0 3 0 0)^0 $J = 12$ parent peaks saturate. The most prominent IR−UV DR rovibronic features are labeled in Figure 5a, which is a higher-sensitivity version of corresponding spectra in Figure 2c of ref 28, Figure 4a of ref 29, and Figure 5 of ref 30. The other IR−UV DR spectra in Figure 5 have (b) 20- and (c) 60-fold increases in IR−UV delay t (and hence z, with fixed $P = 0.20$ Torr). These spectra apparently arise from evolution of collision-induced even-ΔJ RET, as indicated by the assignment grid above trace (c). More significantly, the arrowed $J = 1$ peak at 299.105 nm in trace b is assigned[28] to a P(1) $K' = 1$ transition in the $\tilde{A}-\tilde{X}$ $1_1^0\,3_3^1\,5_0^1$ rovibronic band; this appears to correspond to forbidden odd-ΔJ RET within the (1 0 3 0 0)^0 submanifold from the prepared $J_i = 12$ state to $J_f = 1$. Such a collision-induced ET process has been further

considered in subsequent papers[29,30,32] (but without needing to invoke *a*/*s* nuclear-spin symmetry breaking).

Also of interest in Figure 5b and c is an apparent bandhead (labeled A) of collision-induced features at ~298.5 nm on the short-wavelength edge of the bandhead comprising R(*J*) $K' = 2$ features of the $\tilde{A}-\tilde{X}$ $1_1^0\ 3_3^1\ 5_0^1$ rovibronic band around 298.7 nm. There is experimental evidence[49,50] that bandhead A comprises R(*J*) $K' = 2$ features originating in a rovibronic absorption band tentatively assigned as $\tilde{A}-\tilde{X}$ $1_\#^0\ 2_\#^0\ 3_\#^1\ 4_\#^0\ 5_\#^1$. Here we postulate that the $\tilde{X}\ ^1\Sigma_g^+$ electronic ground state of C_2H_2 includes an additional rovibrational level, designated $(\#\ \#\ \#\ \#\ \#)^\#$, that is, with undetermined zero-order values of each V_i for $i = 1-5$ and of *l*; this level is understood to be IR-dark and nearly isoenergetic with the $(1\ 0\ 3\ 0\ 0)^0$ submanifold. The daggered peak at 298.66 nm in bandhead A has been shown by IR−UV DR studies[49,50] to originate from collision-induced V−V transfer into the $(\#\ \#\ \#\ \#\ \#)^\#$ $J = 16$ state.

A remarkable aspect of Figure 5 that is central to this paper is the collision-induced growth of a quasi-continuous background as the collision number, *z*, increases in traces a−c from approximately zero to 0.66 and then to 1.96, respectively. As in Figure 4, this CIQCB effect is discerned in Figure 5 from the separation between the IR−UV DR signal amplitudes and the dashed horizontal lines that show the levels of scattered UV PROBE light detected by the LIF-sensing photomultiplier in the absence of IR PUMP light. This scattered light level is found to be constant over the range $P = 0-6$ Torr, indicating that Rayleigh scattering of UV PROBE light is negligible from C_2H_2 gas at our sample pressures ($P < 0.5$ Torr). Likewise, the solid horizontal lines show the "zero-light" level with the UV PROBE beam blocked. Assorted tests, such as successive blocking of the IR PUMP and UV PROBE beams, confirm that the CIQCB is a genuine IR−UV DR signal and not a spurious effect (e.g., due to photomultiplier saturation). Moreover, IR−UV DR experiments using a foreign-gas collision partner (presented below) confirm that the kinetics of the quasi-continuous background are truly collision-induced and intramolecular, rather than collision-free (e.g., due to IVR) or arising from intermolecular ET. It should be noted that the CIQCB in Figure 5 has been recorded with a higher signal-to-noise ratio than that in the rapidly scanned survey spectrum at ~322−326 nm in Figure 4; the CIQCB at ~299 nm is effectively constant over the much less extensive UV PROBE wavelength range of Figure 5.

It is particularly significant that the CIQCB signal in Figure 5 can be observed in spectral regions where the UV PROBE is off-resonance from any discrete transitions that originate from IR-bright $(1\ 0\ 3\ 0\ 0)^0$ *J* states. For instance, reference to the relevant atlas of UV-scanned IR−UV DR spectra in Figure 5 of ref 30 shows that the region labeled B around ~298.8 nm in Figure 5c is effectively free of any IR−UV DR features associated with the $(1\ 0\ 3\ 0\ 0)^0$ submanifold itself. This indicates that any IR−UV DR signals detected with the UV PROBE wavelength set in a range such as B must be due to a rovibrational submanifold that is IR-dark and distinct from the IR-bright $(1\ 0\ 3\ 0\ 0)^0$ submanifold.

An important feature of these IR−UV DR experiments is the very low Franck−Condon intensity of the $\tilde{A}-\tilde{X}$ rovibronic bands, either $1_1^0\ 3_3^0\ (4_0\ 6_0)^1$ around ~324 nm (as in Figure 4) or $1_1^0\ 3_3^1\ 5_0^1$ at ~299 nm (as in Figure 5), that are accessed by the UV PROBE.[31,32] This is a disadvantage for some experiments such as direct absorption spectroscopy, but it is advantageous in the present context, where UV-bright states can be projected out of a highly perturbed rovibrational manifold. Very low Franck−Condon factors yield an effectively null baseline against which unusual molecular behavior (e.g., CIQCB and odd-ΔJ ET effects), induced by intramolecular rovibrational perturbations, may become prominent.

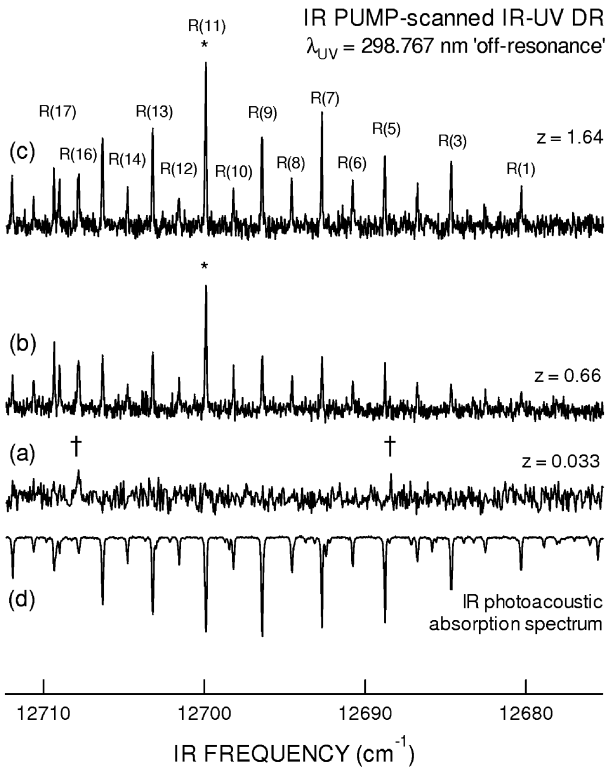

Figure 6. IR PUMP-scanned, LIF-detected IR−UV DR spectra (a−c) in the 12 676 cm^{-1} ($\nu_1 + 3\nu_3$) band of C_2H_2 ($P = 0.20$ Torr, $T = 300$ K) and the UV PROBE wavelength set at an "off-resonance" wavelength of 298.767 nm, away from any discrete rovibrational *J* states of the $(1\ 0\ 3\ 0\ 0)^0$ submanifold.[29] IR−UV delay times *t* and Lennard−Jones collision numbers, *z*, are varied as follows: (a) $t = 10$ ns, $z = 0.033$; (b) $t = 200$ ns, $z = 0.66$; (c) $t = 500$ ns, $z = 1.64$. Trace d is a photoacoustic absorption spectrum, recorded with C_2H_2 pressure $P = 30$ Torr. See the text for further details.

The CIQCB effect in Figure 5 occurs in a UV-scanned IR−UV DR spectrum, but a complementary aspect can also be viewed in the form of IR-scanned IR−UV DR spectra. Such spectra bear out the expectation that IR−UV DR signals should occur irrespective of the UV PROBE wavelength being on or off resonance with discrete rovibrational *J*-states of the $(1\ 0\ 3\ 0\ 0)^0$ submanifold. This is demonstrated in Figure 6 (adapted from Figure 5 in ref 29), where the UV PROBE wavelength is arbitrarily fixed at 298.767 nm, as designated by the asterisked arrow within range B in Figure 5b.

Figure 6a shows a collision-free ($z = 0.033$) IR−UV DR spectrum, which is featureless (apart from a barely discernible pair of IR−UV DR peaks marked by daggers); it shows no parent-type features originating from any *J* state of the IR-bright $(1\ 0\ 3\ 0\ 0)^0$ submanifold with sufficient intensity to account for the abundance of collision-induced IR−UV DR features in the other off-resonance IR−UV DR spectra shown in Figure 6b and c. These other IR−UV DR spectra have (b) 20- and (c) 50-fold increases in IR−UV delay, *t* (and hence *z*, with $P = 0.20$ Torr). Figure 6a−c uses the same instrumental gain, which is set as high as possible to enable detection of these very weak off-resonance IR−UV DR spectra. Moreover, ~60 IR and UV laser shots per data point were used to record Figure 6b and c, a threefold increase in signal-averaging, relative to our usual IR−UV DR measurements,[28−32] including Figures 3−5 above. These IR−UV DR spectra were obtained by scanning the IR

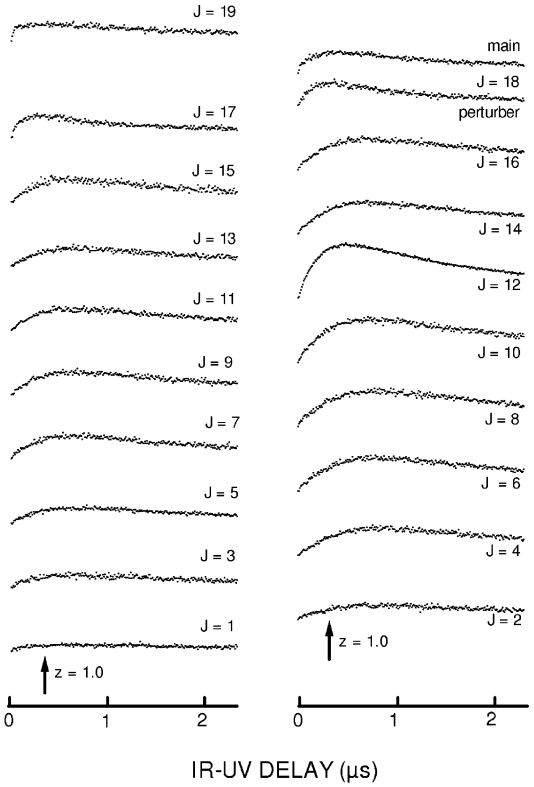

Figure 7. Averaged IR−UV DR kinetic curves for C_2H_2 ($P = 0.20$ Torr), with the UV PROBE set at 298.767 nm, off-resonance from any discrete J states of the $(1\ 0\ 3\ 0\ 0)^0$ submanifold. These represent ET from individual rovibrational $(1\ 0\ 3\ 0\ 0)^0$ J states to CIQCB bath states, with the IR PUMP set to monitor odd-J_i ET (left-hand column) and even-J_i RET (right-hand column) over the range $J_i = 1-19$.

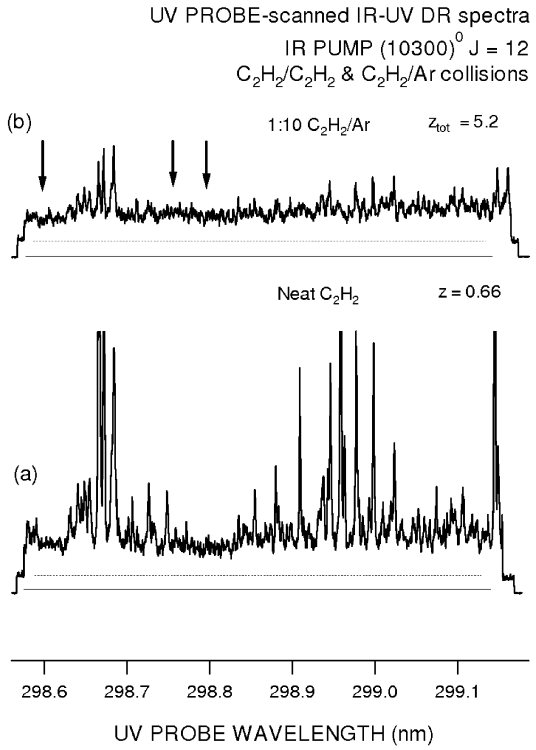

Figure 8. UV-scanned IR−UV DR spectra of C_2H_2 at 300 K, showing CIQCB effects as in Figure 5, with the IR PUMP preparing molecules in the $(1\ 0\ 3\ 0\ 0)^0$ $J_i = 12$ state and the UV PROBE tuned through the $\tilde{A}-\tilde{X}$ $1_1^0\ 3_3^1\ 5_0^1$ band at ~299 nm. Trace a, for neat C_2H_2 with $P_{Ar} = 0$ and $z_{tot} = 0.66$, is identical to Figure 5b. Both traces a and b have $t =$ 200 ns and $P_{C_2H_2} = 0.20$ Torr. Trace b, with $P_{Ar} = 2.0$ Torr and $z_{tot} =$ 1.96, shows the effect of C_2H_2/Ar foreign-gas collisions.

PUMP wavelength though the 12 676 cm^{-1} ($\nu_1 + 3\nu_3$) band of C_2H_2, as indicated by the corresponding photoacoustic reference spectrum shown in trace d.

The asterisked R(11) IR−UV DR feature in Figure 6b and c is a particularly prominent CIQCB peak associated with the $(1\ 0\ 3\ 0\ 0)^0$ $J = 12$ rovibrational state, which appears to serve as the primary gateway for odd-ΔJ collision-induced energy transfer in the $4\nu_{CH}$ manifold of C_2H_2. This state evidently has an exceptionally high collision-induced propensity for population transfer to and from other rovibrational states, notably those that appear to entail forbidden odd-ΔJ RET and/or V−V ET. The asterisked R(11) feature grows in much more efficiently than other collision-induced features in traces b and c. There, even- and odd-J collision-induced IR−UV DR features with $J \neq 12$ all appear prima facie to grow in with comparable efficiencies, yielding a rotational intensity distribution that seems to be quasi-equilibrated (apart from $J = 12$) in trace c with $z =$ 1.64. Closer inspection of Figure 6 suggests that there are other secondary gateways, such as that associated with the R(17) IR−UV DR doublet features in traces b and c with $(1\ 0\ 3\ 0\ 0)^0$ $J =$ 18 "main" and "perturber" rovibrational states, for which the local Coriolis coupling has been assigned recently[54] and IR−UV DR spectra examined in detail.[31]

Similar IR-scanned IR−UV DR spectra are observed with the UV PROBE fixed at other arbitrary off-resonance wavelengths. Of the two weak daggered peaks in trace a, that on the low-wavelength side of the ($\nu_1 + 3\nu_3$)-band R(5) peak decays as z increases in the manner of an ultraweak (but unidentified) parent peak. The other daggered peak coincides (perhaps by accident) with the R(16) peak of the ($\nu_1 + 3\nu_3$) band in traces b−d, which was prominent as an odd-ΔJ collision-induced RET satellite in Figure 3b and c and studied in detail previously.[31] As in other collision-free IR-scanned IR−UV DR spectra recorded under such high gain conditions, we are only rarely able to identify the rovibrational states associated with such weak parent features by fitting to ground-state combination differences.

As in our previous studies,[30−32] IR−UV DR kinetic scans can provide further insight into collision-induced energy transfer, additional to that from IR−UV DR spectra, either UV-scanned as in Figures 4 and 5 or IR-scanned as in Figures 3 and 6. Measurement and processing of IR−UV DR kinetic curves have been discussed elsewhere.[32] Corresponding to Figures 5 and 6, Figure 7 shows a set of IR−UV DR kinetic curves with the UV PROBE set at 298.767 nm, off-resonance from any discrete transitions that originate from J states of the IR-bright $(1\ 0\ 3\ 0\ 0)^0$ submanifold. Kinetic curves recorded under such conditions represent RET and/or V−V ET from individual rovibrational $(1\ 0\ 3\ 0\ 0)^0$ J_i states to CIQCB bath states (and possibly other discrete IR-dark rovibrational submanifolds). Vertical arrows denote the IR−UV delay, t, that corresponds to the Lennard−Jones "gas-kinetic" value of $z = 1.0$. The kinetic curves in Figure 7 are arranged in two columns, with odd-J_i states on the left and even-J_i states on the right. It is notable that the "$J_i =$ 12 to bath" ET gateway channel (labeled "$J = 12$" in the right-hand column of Figure 7) is prominent, with a relatively rapid initial growth rate. Likewise, growth of ET in both main and perturber channels of "$J_i = 18$ to bath" ET is also quite rapid, as observed in the context of Figure 6. Most of the other "J_i to bath" kinetic curves of Figure 7 are uniformly slow to grow, consistent with Figure 6b and c, but in contrast to kinetic curves associated with even-ΔJ RET as in Figure 3 of ref 30, Figure 8 of ref 31, or Figure 2 of ref 32. Figure 7 is part of an extensive

body of IR−UV DR kinetic results (all carefully standardized, signal-averaged, and prepared for self-consistent fitting) that can be simulated by a phenomenological master-equation model.[30−32,49,50] The overall body of IR−UV DR results available for such modeling comprises four sets of experimental kinetic curves, each with the IR PUMP wavelength tuned successively to prepare the $(1\ 0\ 3\ 0\ 0)^0$ rovibrational states with $J_i = 1-19$. We have reported three of these kinetic data sets previously (sets A − C), in which the UV PROBE was tuned to wavelengths at ∼299 nm characteristic of the $(1\ 0\ 3\ 0\ 0)^0$ $J_f = 1$ (set A),[30] $J_f = 12$ (set B),[32] and $J_f = 17$ (set C).[31] Figure 7 represents the fourth kinetic data set (set D), in which the UV PROBE is set to off-resonance from any discrete IR−UV DR feature, to sample the kinetics of the accompanying CIQCB bath.

The efficiency of collision-induced transfer into the quasi-continuum can be inferred tentatively on the basis of the kinetic master equation model that is considered in detail elsewhere.[49,50] For instance, this model indicates that a C_2H_2/C_2H_2 self-collisional state-to-state rate coefficient of 0.3 μs^{-1} $Torr^{-1}$ (9.3×10^{-12} cm^3 $molecule^{-1}$ s^{-1}) suffices to reproduce the observed "$J_i = 12$ to bath" transfer kinetics from the $(1\ 0\ 3\ 0\ 0)^0$ $J_i = 12$ level to the CIQCB bath; this corresponds to less than 2% of the Lennard−Jones gas-kinetic rate coefficient and is approximately 12 times less efficient than $\Delta J = \pm 2$ RET at $J_i = 12$.

As in our original IR−UV DR investigation of the $4\nu_{CH}$ manifold of C_2H_2,[28] we have measured the effect of foreign-gas collisions on CIQCB IR−UV DR signals. We have examined C_2H_2 diluted in argon (Ar), for which we define a total collision number, z_{tot}, at IR−UV delay, t (e.g., in units of μs), as follows

$$z_{tot} = z_{C_2H_2} + z_{Ar} = [k_{LJ}(C_2H_2)\, P_{C_2H_2} + k_{LJ}(Ar)\, P_{Ar}]\, t \quad (1)$$

where z_M, $k_{LJ}(M)$, and P_M are collision numbers, Lennard−Jones collisional rate constants (e.g., in units of μs^{-1} $Torr^{-1}$), and partial pressures (e.g., in units of Torr), respectively, for gas-mixture components $M = C_2H_2$ or Ar. (For M = Ar at 300 K, we take $k_{LJ} = 11.3\ \mu s^{-1}\ Torr^{-1} = 3.51 \times 10^{-10}$ cm^3 $molecule^{-1}$ s^{-1}; see Section I for corresponding $M = C_2H_2$ self-collisional values.[22])

Figure 8 shows two UV-scanned IR−UV DR spectra, recorded with $t = 200$ ns, $P_{C_2H_2} = 0.20$ Torr, and $T = 300$ K in (a) neat C_2H_2 gas ($P_{Ar} = 0$, $z_{tot} = 0.66$) and (b) a 1:10 C_2H_2/Ar mixture ($P_{Ar} = 2.0$ Torr, $z_{tot} = 1.96$). As in Figure 5, the IR PUMP is tuned to prepare the $(1\ 0\ 3\ 0\ 0)^0$ $J_i = 12$ rovibrational state as the UV PROBE scans the 299-nm $\tilde{A}-\tilde{X}$ $1_1^0\ 3_3^1\ 5_0^1$ rovibronic band; the spectra in Figures 5b and 8a are identical. The CIQCB effect is again distinguished from other IR−UV DR spectroscopic features in Figure 8 by dashed horizontal lines showing levels of scattered UV PROBE light in the absence of IR PUMP light and solid horizontal lines showing the "zero-light" level with UV PROBE beam blocked. It is noteworthy that the IR−UV DR background amplitude in Figure 8b, underlying the sharper discrete (and often assignable) spectral features, is virtually independent of the UV PROBE wavelength. Moreover, there are no localized regions of the UV-scanned spectrum where the continuous background amplitude appears to be markedly enhanced by the addition of Ar. Additional IR−UV DR measurements at even longer delays, t, than those in Figure 8 (e.g, $t = 0.6$ μs, $z_{tot} = 15$ for the same 1:10 C_2H_2/Ar mixture), the UV-scanned IR−UV DR spectrum collapses to an effectively constant background amplitude devoid of any discrete structure and independent of the UV PROBE wavelength used to observe it. These results reflect the rovibrationally averaged, quasi-continuous nature of the background signal and the overall mechanism by which the CIQCB bath states appear to be populated and equilibrated.

Quantitative comparison of the relative amplitudes of the CIQCB signal in Figure 8a and b is complicated by two collision-dependent phenomena: quenching of LIF intensity and the balance between beam flyout and diffusion mass-transport effects.[32,49] Quenching of fluorescence from the $\tilde{A}\ ^1A_u$ electronically excited manifold of C_2H_2 has been characterized previously,[32] leading us to expect that C_2H_2/Ar collisions would cause the LIF-detected IR−UV DR signal amplitude observed in Figure 8b to be attenuated by a factor of at least 3 relative to the conditions of Figure 8a, at all IR−UV delays, t. Mass-transport effects, as considered previously,[32] comprise a tradeoff between beam flyout (predominant in the low-P, short-t limits) and diffusion (relevant at higher pressures, P, and/or longer values of IR−UV delay, t); in the former case, molecules escape relatively readily from the zone where they are excited and from which their fluorescence is collected, whereas diffusion tends to contain state-selected molecules in the LIF viewing zone for a longer time interval. Addition of Ar is therefore expected to partially offset the attenuating effect of LIF quenching at longer IR−UV delays, t.

Arrows in Figure 8b designate three off-resonance UV PROBE wavelengths: (a) 298.767 nm, (b) 298.803 nm, and (c) 298.604 nm. All are in regions free of any discrete IR−UV DR features associated with J states of the $(1\ 0\ 3\ 0\ 0)^0$ submanifold. These UV PROBE wavelengths were used to record the three pairs of IR−UV DR kinetic curves shown in Figure 9, with the IR PUMP fixed on the $(\nu_1 + 3\nu_3)$-band R(11) peak, preparing the $(1\ 0\ 3\ 0\ 0)^0$ $J_i = 12$ state. The upper curve in each pair is for neat C_2H_2 ($P_{C_2H_2} = 0.10$ Torr), while the lower curve is for a 1:10 C_2H_2/Ar mixture ($P_{C_2H_2} = 0.10$ Torr, $P_{Ar} = 1.0$ Torr); the arrows in Figure 9 show values of t at which $z_{tot} = 1.0$. The similarity between the kinetic curves of the upper traces (neat C_2H_2) in Figures 9a−c should be noted. This is consistent with the previously recognized uniformity of temporal growth and decay of the background signal, irrespective of UV PROBE wavelength, and is relevant to our kinetic master-equation modeling.[49,50] We note that, in the early part (e.g., $t < 0.3$ μs) of each pair of kinetic curves in Figure 9, differences in mass-transport effects have little effect on relative signal amplitude so that LIF quenching by Ar is the only additional effect that needs to be considered in comparing IR−UV DR signals for neat C_2H_2 and C_2H_2/Ar mixtures. Furthermore, the initial growth of the lower traces (1:10 C_2H_2/Ar) in Figure 9a−c is appreciably faster than that for the upper traces (neat C_2H_2) in each section (particularly if the lower curves are adjusted by a factor of 3 to compensate for C_2H_2/Ar collisional quenching).

It is particularly remarkable that the kinetic curves in Figure 9, showing the growth and decay of the CIQCB signal, reach their maximum value within an IR−UV delay interval corresponding to $z = 1$ in the case of neat C_2H_2 and to $z_{tot} = 5$ with 1:10 C_2H_2/Ar mixtures. This implies that the corresponding transfer efficiencies are much higher than would be expected for simple thermal equilibration (e.g., by vibration-to-translation/rotation energy transfer).[1−7] As will be discussed in Section IV below, such kinetics are consistent with collision-induced intramolecular V−V energy transfer. Figures 8 and 9 have significant mechanistic implications, concerning the CIQCB bath kinetics (whether they are collision-induced and, if so, intramolecular or intermolecular), as discussed in Section IV below.

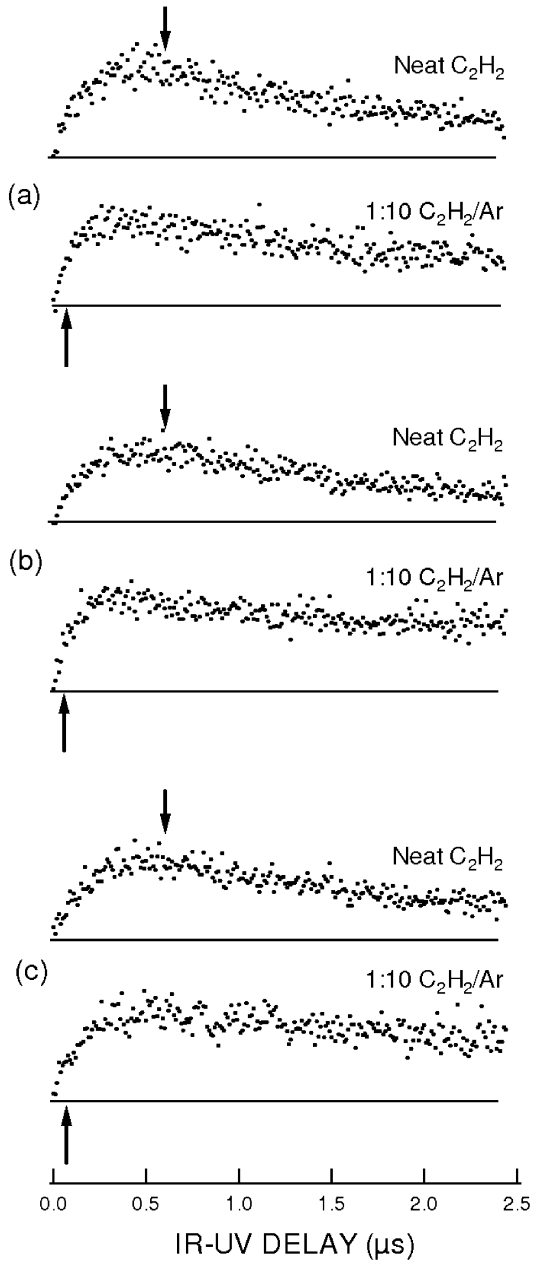

Figure 9. Pairs of IR−UV DR kinetic curves for neat C_2H_2 and a 1:10 C_2H_2/Ar mixture with $P_{C_2H_2} = 0.10$ Torr, $T = 300$ K, and arrows indicating $z_{tot} = 1.0$. The IR PUMP is set to prepare the $(1\ 0\ 3\ 0\ 0)^0$ $J_i = 12$ state and the UV PROBE is set at three arbitrary off-resonance wavelengths to probe the CIQCB bath as designated by the arrows in Figure 8b: (a) 298.767 nm; (b) 298.803 nm; (c) 298.604 nm.

IV. Mechanistic Questions: CIQCB Effects

The results presented in Sections II and III reinforce the conclusions of our previous IR−UV DR studies of the $4\nu_{CH}$ manifold of C_2H_2,[29−32] particularly concerning the concept that discrete features in the collision-induced kinetics of IR−UV DR spectra assigned to the IR-bright $(1\ 0\ 3\ 0\ 0)^0$ submanifold are accompanied by underlying signals from a ubiquitous long-lived CIQCB bath (e.g., as depicted in Figure 2) as well as other discrete IR-dark/UV-bright rovibrational submanifolds. A key outcome of this paper is evidence that such an IR-dark/UV-bright collision-induced IR−UV DR background accounts predominantly for many of the unexpected observations in our IR−UV DR measurements, such as collision-induced satellites that seem to arise from odd-ΔJ RET and/or V−V ET; these are formally forbidden in vibrational states with well-defined vibrational angular momentum $l = 0$, but may become allowed[27,29−32] in the presence of intramolecular perturbations that spoil l as a good quantum number and allow l doublets to occur for each value of J, without invoking breaking of *a*/*s* nuclear-spin symmetry that entails (unlikely) interconversion of ortho and para nuclear-spin modifications of C_2H_2.

For instance, odd-ΔJ ET processes, such as those represented by IR−UV DR kinetic curves for "even J_i to $J_f = 17$" in Figure 8 of ref 31 and "odd J_i to $J_f = 12$" in Figure 2 of ref 32 can be entirely attributed to the CIQCB bath. Moreover, as indicated in Section 2, the unexpectedly slow decay of the $(\nu_1 + 3\nu_3)$-band R(11) parent feature in the IR-scanned IR−UV DR spectra of Figure 3b and c is explained by an increasing contribution (as t and z increase) from the CIQCB bath signal that underlies regular IR−UV DR signals from the directly probed IR-bright $(1\ 0\ 3\ 0\ 0)^0$ rovibrational state with $J_i = J_f = 12$. Similar interpretations[32,49] apply to the IR-scanned IR−UV DR spectra with $J_f = 17$ in Figures 6 and 7 of ref 31.

In further experiments,[49,50] we have observed CIQCB effects via UV-scanned IR−UV DR spectra with the IR PUMP preparing the $(1\ 0\ 3\ 0\ 0)^0$ $J_i = 12$ state and the UV PROBE tuned in the $\tilde{A}-\tilde{X}$ $1_1^0\ 2_0^1\ 3_3^0\ 5_0^1$ rovibronic band at ∼296 nm, in addition to those at ∼324 nm in Figure 4 and at ∼299 nm in Figure 5. Likewise, we have recorded other IR-scanned IR−UV DR spectra[49,50] with the UV PROBE at ∼323.32 nm and $z = 0.66$. As the UV PROBE is tuned away in discrete 0.001-nm steps from resonance with the $(1\ 0\ 3\ 0\ 0)^0$ $J_i = 17$ state, the amplitude of IR−UV DR parent and even-ΔJ satellite features collapse markedly, whereas accompanying apparent odd-ΔJ ET satellites do not; this confirms that collision-induced odd-ΔJ features observed in such spectra arise predominantly from the CIQCB bath signal.

The observed IR−UV DR kinetics for prepared $(1\ 0\ 3\ 0\ 0)^0$ J_i states can therefore be treated as a superposition of concurrently monitored transfer to the CIQCB bath (with a quasi-continuous UV PROBE spectrum) as well as more conventional ET processes for $(1\ 0\ 3\ 0\ 0)^0$ states with well-defined values of J_f (and discretely structured UV PROBE spectra). This enables the background signal contribution of IR−UV DR intensity originating from the IR-dark bath to be subtracted from such kinetic curves, to separate the concurrent processes in readiness for modeling of the kinetics.[31,32,49,50] In the meantime, a few key mechanistic questions need to be addressed, as follows.

Are the CIQCB and Odd-ΔJ Signals due to Collision-Induced Intramolecular Processes? There are three possible mechanisms to which the CIQCB kinetics, observed in the context of Figures 8 and 9, might be tentatively attributed: (i) collision-free intramolecular vibrational redistribution (IVR); (ii) collision-induced intramolecular RET and/or V−V ET to a quasi-continuous bath; (iii) collision-induced intermolecular exchange of rovibrational energy with a quasi-continuous bath. We expect the population of states by mechanism i via collision-free IVR-type processes (which are common in large polyatomic molecules with highly congested vibrational or vibronic manifolds)[10,15−17] to be insensitive to addition of a foreign-gas collision partner such as Ar. Likewise, collision-induced intermolecular ET, as in mechanism iii, should depend only on C_2H_2/C_2H_2 collisions and not on C_2H_2/Ar collisions.[5,6] Mechanisms i and iii are therefore inconsistent with the fact that CIQCB signals for C_2H_2/Ar gas mixtures in Figures 8b and 9 are relatively strong, especially when we take account of the threefold attenuation expected from LIF quenching and the containment of state-selected molecules in the LIF viewing zone by diffusion-type mass transport. The faster initial growth of

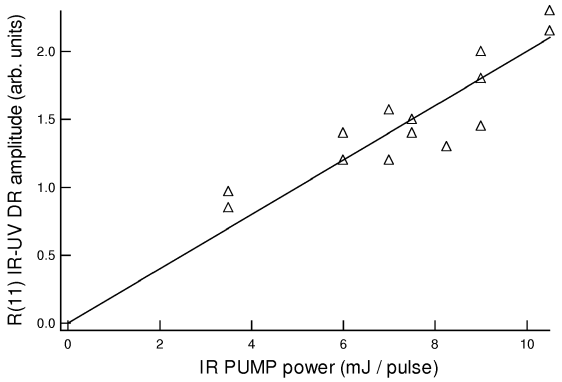

Figure 10. R(11) IR−UV DR background signal strength for C_2H_2 ($P = 0.20$ Torr, $t = 550$ ns, $z = 1.8$) plotted as a function of IR PUMP power. The IR PUMP is set to prepare the $(1\ 0\ 3\ 0\ 0)^0$ $J_i = 12$ state and the UV PROBE is at an arbitrary off-resonance wavelength (298.767 nm, as asterisked in Figure 5).

each lower trace (1:10 C_2H_2/Ar) in Figure 9a−c as well as the comparable relative magnitudes of each pair of kinetic curves are also inconsistent with mechanisms i and iii but consistent with collision-induced intramolecular ET, as in mechanism ii. As in previous studies,[5,6] we therefore attribute the primary mechanism that populates the CIQCB bath to a collision-induced intramolecular process in which the same molecule is initially state-selected and finally LIF-detected after collision-induced ET. In addition, we have made IR−UV DR kinetic measurements[49] of the $(\nu_1 + 3\nu_3)$-band R(11) background signal (asterisked in Figure 6) for neat C_2H_2 over a range of pressure up to 0.4 Torr; here too, the observed pressure dependence is consistent with the collision-induced intramolecular mechanism ii.

Is a Multiphoton or Multiple-Photon Excitation Mechanism Likely? To rationalize the CIQCB signals and their associated complexity, we have considered the possibility that focusing the IR PUMP in the sample might yield some form of coherent or sequential two-photon excitation mechanism. Such a mechanism, if valid, might be expected to raise state-selected C_2H_2 molecules to initial rovibrational states $(V, J, K)_i$ with sufficient energy (>25 400 cm^{-1}) to be chemically significant (e.g., well above the ∼15 000 cm^{-1} threshold for formation of vinylidene,[40−47]) and with a much higher density of states than in the single-photon IR excitation scheme shown in Figure 1. In an IR−UV DR scheme involving two-photon IR excitation, it is anticipated that UV PROBE excitation of C_2H_2 at ∼300 nm would access its $\tilde{A}\ ^1A_u/\tilde{B}\ ^1B_u$ vibronically excited manifold above ∼25 400 cm^{-1} and might thereby generate fluorescence from either C_2H_2 (via diffuse high-energy vibronic states)[55] or C_2H (by photopredissociation).[56] With the possibility of such an excitation scheme in mind, we have investigated the dependence of the $(1\ 0\ 3\ 0\ 0)^0$ $J_i = 12$ IR−UV DR background signal (as observed in Figure 5) on IR PUMP power. Figure 10 was recorded for C_2H_2 ($P = 0.20$ Torr, $t = 550$ ns, $z = 1.8$) with the IR PUMP fixed on the $(\nu_1 + 3\nu_3)$-band R(11) peak and the UV PROBE fixed at an arbitrary off-resonance wavelength (299.767 nm, asterisked in Figure 5b); each data point was averaged over ∼20 laser shots. A linear fit is obtained over a factor-of-three range of IR PUMP powers, which is inconsistent with the nonlinear power dependence usually expected of coherent multiphoton excitation. The proportionality of R(11) IR−UV DR background signal strength to IR PUMP power is also inconsistent with a possible CIQCB mechanism involving Stark-induced mixing of rovibrational states of the $(1\ 0\ 3\ 0\ 0)^0$ submanifold, effectively induced by the electric field of the IR PUMP laser. (In contrast, we note studies of the vibrational Stark effect in C_2H_2,[57] in which the transition strength of nominally forbidden rovibrational transitions, induced by laser field-induced Stark mixing, is shown to vary in a nonlinear fashion with the strength of the applied laser field.)

The linear power dependence in Figure 10, although inconsistent with coherent two-photon IR absorption, does not necessarily rule out the possibility that rovibrational states $(V, J, K)_i$ of the $\tilde{X}\ ^1\Sigma_g^+$ manifold around 25 400 cm^{-1} are populated by sequential two-step IR excitation. Such an IR−IR−UV triple resonance scheme might conceivably give rise to the CIQCB signal by collision-induced ET to other high-lying rovibrational states detected by the UV PROBE over a wide, quasi-continuous range. However, the IR−IR−UV mechanism is considered unlikely for a number of reasons. In particular, it would require a rare spectroscopic accident for two rovibrational transitions to share a common intermediate state, let alone allow the background signal to be independently observed when pumping each J state of the $(1\ 0\ 3\ 0\ 0)^0$ submanifold in turn, as in Figure 6. Two-photon IR excitation schemes (either coherent or sequential) are therefore regarded as implausible in this context.

We note that O'Brien et al.[58] have observed a "quasi-continuous baseline" by dispersed LIF into the $\tilde{X}\ ^1\Sigma_g^+$ manifold of C_2H_2 over the internal-energy range 6000−20 000 cm^{-1}, following single-photon Q(1) $K' = 1$ UV excitation of the $\tilde{A}-\tilde{X}$ $3_0^2\ K_0^1$ rovibronic absorption band at ∼226 nm. The effect has been observed with C_2H_2 sample pressures in the range $P = 1-9$ Torr, corresponding to collision numbers $z = 3-30$ during the fluorescence lifetime, and also under collision-free conditions in a molecular beam.[58] The most likely source of this effect is considered to be UV multiphoton absorption that could result in luminescence from C_2H or C_2 photofragments.[58] Some aspects of the CIQCB effect in our IR−UV DR experiments might well be ascribed to a similar mechanism involving multiphoton excitation of rovibrational-state-selected C_2H_2 molecules by the UV PROBE radiation. However, our CIQCB effect is observed at relatively low collision numbers (e.g., $z = 0.66$ as in Figures 5b and 6b) but it is not discernible under collision-free conditions (e.g., $z = 0.033$ as in Figures 5a and 6a). Moreover, a UV multiphoton excitation mechanism cannot explain the occurrence of collision-induced odd-ΔJ RET and/or V−V ET satellites in IR−UV DR spectra, observed in the $4\nu_{CH}$ region of C_2H_2 and understood to be associated with the CIQCB. In addition, prolonged experimental runs yielded no discernible diminution of IR−UV DR signal amplitude or sample pressure that might be attributable to dissociation of C_2H_2 by the UV PROBE laser, although minute traces of decomposition products built up on sample cell windows and walls over several months of IR PUMP and UV PROBE irradiation of C_2H_2.

What is the Most Likely Source of the CIQCB Quasi-Continuum? In view of the above discussion of possible mutiphoton excitation processes, the source of the quasi-continuous background in collision-induced IR−UV DR spectra such as Figures 4 and 5 remains an open question. Two plausible classes of mechanism are illustrated schematically in Figure 11: (a) collision-induced ET to a quasi-continuous IR-dark rovibrational manifold of $(V, J, K)_f$ states, as depicted previously in Figure 2; (b) UV PROBE transitions from ET-populated discrete IR-dark rovibrational states $(V, J, K)_f$ to an electronically excited quasi-continuum labeled (V', J', K'), not necessarily belonging to the $\tilde{A}\ ^1A_u$ manifold of C_2H_2. In each case, sequential IR−UV DR excitation can reveal irregular, interesting aspects of molecular behavior.

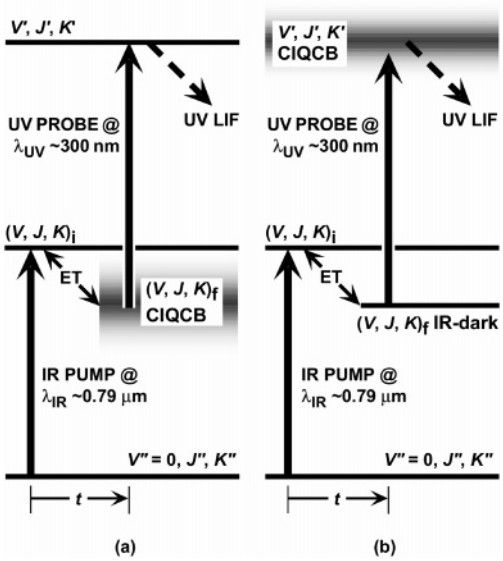

Figure 11. Two possible mechanisms for CIQCB bath effects in IR−UV DR excitation schemes: (a) rovibrational quasi-continuum (as in Figure 2); (b) rovibronic quasi-continuum.

On the basis of our IR−UV DR experiments, postulated mechanisms as in Figure 11a are favored relative to those in Figure 11b. As mentioned above, an electronically excited quasi-continuum as in Figure 11b cannot by itself explain the occurrence of collision-induced odd-ΔJ RET and/or V−V ET satellites that are associated with the CIQCB observed in IR−UV DR spectra of the $4\nu_{CH}$ region of C_2H_2. Moreover, our results appear to be consistent with regular IR−UV DR excitation of $\tilde{A}-\tilde{X}$ fluorescence from C_2H_2 itself, rather than excitation of luminescence from a photofragment such as C_2H or C_2 or another (unidentified) electronic state of C_2H_2. It is therefore considered likely[49] that the CIQCB signal arises predominantly from collision-induced ET into a bath of levels that are close to the $(1\ 0\ 3\ 0\ 0)^0$ submanifold, as depicted schematically in Figures 2 and 11a. The IR−UV DR background signal from lower-lying levels will decline with increasing energy defect, so that UV PROBE transitions from bath levels in each spectral region should terminate in the same upper vibronic levels (i.e., ν_4'/ν_6', $\nu_2' + \nu_5'$, or $\nu_3' + \nu_5'$) as those used to probe the $(1\ 0\ 3\ 0\ 0)^0$ submanifold via corresponding $\tilde{A}-\tilde{X}$ vibronic bands, namely, $1_1^0\ 3_3^0\ (4_0\ 6_0)^1$ at ~324 nm, $1_1^0\ 3_3^1\ 5_0^1$ at ~299 nm, and $1_1^0\ 2_0^1\ 3_3^0\ 5_0^1$ at ~296 nm.[31]

To rationalize the CIQCB effects observed in our IR−UV DR experiments, we postulate the existence of an IR-dark/UV-bright quasi-continuous rovibrational bath that is close (in terms of internal energy) to the $4\nu_{CH}$ region of C_2H_2 at ~12 700 cm^{-1} and accessible by collision-induced ET from discrete IR-bright rovibrational states of the $4\nu_{CH}$ manifold, notably those of the $(1\ 0\ 3\ 0\ 0)^0$ submanifold. However, the origin of any such quasi-continuum is not at all obvious. Single-photon IR excitation of the $4\nu_{CH}$ manifold of C_2H_2 at ~12 700 cm^{-1} is below the internal energy range that is chemically significant (e.g., the threshold above 15 000 cm^{-1} for isomerization to vinylidene[40−47]) so that a genuinely diffuse rovibrational continuum due to processes such as predissocation seems improbable.

We understand that the CIQCB is due to a congested assembly of discrete C_2H_2 rovibrational states, many of them IR-dark, that are extensively coupled by various intramolecular perturbations (e.g., anharmonic mixing, *l*-resonance effects, and Coriolis coupling). A quasi-continuous IR−UV DR background signal is likely to arise via an accumulation of intensity from many weak, overlapping IR−UV DR features that cannot be resolved adequately with our UV PROBE optical bandwidth (typically 0.2−0.3 cm^{-1} from an excimer-pumped tunable dye laser[30]). A quasi-continuous IR−UV DR background signal (presumably associated with regions of the $\tilde{A}-\tilde{X}$ absorption system) does not necessarily indicate the existence of genuine continuum structure in the region of the $\tilde{X}\ ^1\Sigma_g^+$ manifold that is monitored in our LIF-detected IR−UV DR measurements. (Incidentally, we note indications of localized diffuse or quasi-continuous absorption in $\tilde{A}-\tilde{X}$ spectra of C_2H_2 originating from the $V'' = 0$ and $V''_4 = 1$ vibrational levels of the $\tilde{X}\ ^1\Sigma_g^+$ manifold, measured with ~0.2 cm^{-1} resolution.[59]).

The origin of the quasi-continuous IR−UV DR background signal is supposed to arise as the IR−UV delay, *t*, and hence the collision number, *z*, increases and an increasing fraction of the initial rovibrational population prepared by the IR PUMP redistributes and rotationally equilibrates into the many rovibrational states (most of them IR-dark) that make up the quasi-continuous bath. The fractional population in each individual level of the bath, relative to that initially prepared by the IR PUMP, is likely to be very small at all IR−UV delays (e.g., discrete IR−UV DR peaks remain prominent in Figure 5b and c, recorded with $z = 0.66$ and $z = 1.96$, respectively). However, LIF detection of such small fractional populations in the bath will be facilitated by the exceptionally high UV brightness that we postulate for many IR-dark/UV-bright bath states. At arbitrary UV PROBE wavelengths (and likewise as the UV PROBE is tuned continuously), we expect that many UV-bright $\tilde{A}-\tilde{X}$ rovibronic absorption transitions (originating from the bath) will fall within the optical bandwidth of the UV PROBE.

We have also considered the possibility that electronically excited triplet ($S = 1$) states of C_2H_2 might be implicated in our observations. There is an extensive body of literature, both experimental[60−62] and theoretical,[63] on singlet−triplet interactions in C_2H_2. Two pairs (T_1 and T_2, respectively) of cis- and trans-bent isomers have been identified: $\tilde{a}\ ^3B_2$ and $\tilde{b}\ ^3B_u$, and $\tilde{c}\ ^3A_u$ and $\tilde{d}^3A_2$, in order of increasing energy; these all lie above 28 500 cm^{-1} and are therefore inaccessible to either one- or two-photon excitation within the S_0 (linear, $\tilde{X}\ ^1\Sigma_g^+$) electronic ground state of C_2H_2 by IR PUMP radiation at ~12 700 cm^{-1}. There is evidence[63] that a higher-energy triplet state, T_3 (trans-bent, $\tilde{e}^3B_u$), of C_2H_2 can overlap and interact perturbatively with the S_1 (trans-bent, $\tilde{A}\ ^1A_u$) electronic singlet ($S = 0$) state that fluoresces after UV PROBE excitation at ~296 nm, ~299 nm, or ~323 nm in our IR−UV DR experiments.[28−32] In particular, intersystem crossing between specific rovibronic levels of T_3 and the $V'_3 = 3$ S_1 manifold at ~45 300 cm^{-1} (below the dissociation limit[64] $D_0 = 46\,074$ cm^{-1} and the onset of predissociation) have been characterized in detail recently,[61] following earlier observations of related effects.[60] The levels of rovibronic excitation used in our IR−UV DR experiments[28−32] are in the ranges 43 500−44 000 cm^{-1} (with the UV PROBE at ~323 nm) and 46 000−46 500 cm^{-1} (with the UV PROBE at ~296−299 nm). These fall in the energy region where intersystem crossing and predissociation are active, but we cannot discern any obvious CIQCB mechanism (e.g., as in Figure 11b) that might arise from singlet−triplet interactions between the S_1 and T_1, T_2, or T_3 manifolds.

Is the $4\nu_{CH}$ Rovibrational Manifold Sufficiently Dense to Explain the CIQCB? The foregoing proposed CIQCB mechanism requires a sufficiently high density of UV-bright rovibrational states in the bath to be populated by collision-induced transfer, after initial IR PUMP excitation, to yield a quasi-continuous UV-scanned absorption spectrum in which many

bath states are monitored simultaneously at any arbitrary UV PROBE wavelength. We have used established methods[65] to estimate the number of vibrational levels in $\tilde{X}\ ^1\Sigma_g^+$ polyads or clusters with pseudo-quantum number $n_{res} = 5V_1 + 3V_2 + 5V_3 + V_4 + V_5 = 20$. The predicted distribution of Σ^+, Π, Δ, and Φ (i.e., $l = 0-4$) vibrational levels, both *gerade* and *ungerade*, in C_2H_2 with $n_{res} = 20$ has a maximum density of ~1 level per cm^{-1} with a full width at half-maximum of ~500 cm^{-1}.[49] Cascaded mixing of vibrational angular momentum, *l*, by Coriolis coupling and *l*-resonance effects is considered to be feasible over such a range of $l = 0-4$. In addition, collision-induced RET that inevitably accompanies V−V ET will cause the estimated density of available *J*-resolved rovibrational states to be 1−2 orders of magnitude greater than the "RET-free" density of vibrational levels. It is then plausible for the effective density of IR-dark/UV-bright rovibrational states to exceed 10 states per cm^{-1}. This yields substantially congested collision-induced IR−UV DR spectra, such that several rovibronic transitions at ~299 nm consistently fall within the optical bandwidth (0.2−0.3 cm^{-1}, typically[30]) of the UV PROBE laser, irrespective of its wavelength. This density may also suffice to yield a CIQCB when IR-scanned IR−UV DR spectra are observed with a narrower UV PROBE optical bandwidth (~0.06 cm^{-1}) at ~323 nm.[49,53]

V. Concluding Discussion

It is remarkable that a supposedly simple polyatomic molecule such as C_2H_2, with its linear, nondipolar, tetratomic, centrosymmetric structure, can give rise to a highly complicated variety of dynamical processes, even at internal energies of its ground electronic state that are too low to be regarded as chemically significant. Much of this complexity can be understood, at least qualitatively, in terms of a rich assortment of perturbations (notably anharmonic, *l*-resonance, and Coriolis coupling) that can influence both intramolecular and collision-induced state-to-state rovibrational energy transfer processes. Within this context, our IR−UV DR spectroscopic experiments on C_2H_2 in its 12 700-cm^{-1} $4\nu_{CH}$ rovibrational manifold[28−32] have revealed a fascinating collision-induced quasi-continuous background (CIQCB), which appears to be associated with unexpected odd-ΔJ energy-transfer channels.

In this paper, we have consolidated evidence of the CIQCB effect in C_2H_2 and examined its likely mechanistic origins. In particular, Figure 7 shows a set of IR−UV DR kinetic curves, each recorded with the IR PUMP wavelength tuned to prepare specific *J*-states of the $(1\ 0\ 3\ 0\ 0)^0$ level in the $\tilde{X}\ ^1\Sigma_g^+$ electronic ground state, but with the UV PROBE set at an off-resonance wavelength (298.767 nm, well away from any discrete rovibronic feature in the LIF-detected spectrum of the $\tilde{A}-\tilde{X}\ 1_1^0\ 3_3^1\ 5_0^1$ vibronic band). UV-scanned and IR-scanned IR−UV DR spectra, as in Figures 5 and 6, respectively, are consistent with the IR−UV DR kinetic curves of Figure 7. Likewise, Figures 8 and 9 show the effects of collisions between C_2H_2 and a foreign-gas partner (Ar), thereby confirming that the collision-induced processes responsible for the CIQCB are intramolecular rather than intermolecular.

The off-resonance "J_i to CIQCB bath" IR−UV DR kinetics revealed by Figure 7 are mechanistically significant[29,32,49,50] in that they account entirely for odd-ΔJ rovibrational energy transfer that is observed in the IR−UV DR kinetics for "J_i to $J_f = 12$" and "J_i to $J_f = 17$" transfer, as reported respectively in Figure 2 of ref 32 and Figure 8 of ref 31; they also partially account for the odd-ΔJ ET observed in IR−UV DR kinetics for "J_i to $J_f = 1$" transfer, as in Figure 3 of ref 30. In all three cases ("J_i to $J_f = 1$, 12, and 17"), both even-ΔJ and odd-ΔJ, the "J_i to CIQCB bath" kinetics as in Figure 7 accounts for long-lived tails that are much slower to decay to zero than expected for regular RET.[32,49,50] Moreover, the "J_i to CIQCB bath" IR−UV DR kinetics varies little as the off-resonance UV PROBE wavelength is varied (e.g., compare Figure 9a−c), so that Figure 7 can be treated as a representative sample of such kinetics, both on and off resonance, at all UV PROBE wavelengths in the vicinity of ~299 nm. We are therefore able to regard the overall kinetics as a superposition of the off-resonance "J_i to CIQCB bath" kinetics on the corresponding sets of on-resonance discrete-J_f IR−UV DR kinetics, and to subtract the former from the latter in order to enable master-equation modeling of regular RET and V−V ET kinetics. This separation of concurrent processes facilitates detailed analysis of the three sets of on-resonance discrete-J_f IR−UV DR kinetic curves ("J_i to $J_f = 1$, 12, and 17"), that is, as in Figure 3 of ref 30, Figure 2 of ref 32, and Figure 8 of ref 31.[32,49,50]

On the basis of issues discussed in Section IV above, we postulate that the CIQCB phenomenon arises as depicted schematically in Figures 2 and 11a. Its primary source is understood to be collision-induced ET after IR PUMP excitation to a congested array of IR-dark/UV-bright $\tilde{X}\ ^1\Sigma_g^+$ rovibrational states from polyads or clusters with $n_{res} = 20$, to which the $(1\ 0\ 3\ 0\ 0)^0$ level in particular and the $4\nu_{CH}$ manifold in general belong, followed by LIF-detected UV PROBE $\tilde{A}-\tilde{X}$ rovibronic absorption. Many approximately isoenergetic rovibrational states above 12 700 cm^{-1} may contribute to the CIQCB. We estimate that the effective density of available IR-dark/UV-bright rovibrational states in the CIQCB exceeds 10 states per cm^{-1}, on the basis of all $n_{res} = 20$ vibrational levels with $l = 0-4$ (Σ^+, Π, Δ, and Φ), both gerade and ungerade, enhanced by 1−2 orders of magnitude via collision-induced RET. The UV PROBE optical bandwidths employed (typically ~0.25 cm^{-1}) then yield a quasi-continuous distribution of rovibrational states, consistent with the observed CIQCB effects. An empirical model of the CIQCB, based on observed IR−UV DR kinetics as in Figure 7, is used together with a phenomenological master-equation model of the RET and V−V ET kinetics of discretely identified (*V*, *J*, *K*) states.[32,49,50] Significantly, the $l > 0$ (Π, Δ, Φ, ...) character of rovibrational states contributing to the CIQCB will cause *J* states to occur in *l*-type doublets with *e* and *f* symmetry components.[51] This is then expected to allow collision-induced rovibrational transfer ($e \leftrightarrow f$) with odd ΔJ as well as even ΔJ, without needing to invoke *a*/*s* nuclear-spin symmetry breaking or (usually forbidden) interconversion of ortho and para nuclear-spin modifications of C_2H_2.[29,30]

Our collision-induced IR−UV DR kinetic studies also indicate the importance of *J*-specific energy-transfer gateways, a concept that is familiar in collision-induced electronic[66] and vibrational transfer,[67] as well as in the dynamics of IVR[16] and unimolecular reactions.[68] IR−UV DR mechanisms for C_2H_2 in its 12 700 cm^{-1} $4\nu_{CH}$ rovibrational manifold are understood to involve discrete IR-dark/UV-bright rovibrational gateway states that are nearly isoenergetic with the discrete IR-bright rovibrational states and the CIQCB bath states. The most prominent of these rovibrational states, $(1\ 0\ 3\ 0\ 0)^0$ $J_i = 12$, has been recognized as a primary gateway for unusually complicated odd-ΔJ $(1\ 0\ 3\ 0\ 0)^0$ "J_i to $J_f = 1$" transfer kinetics.[29−32,49,50] In addition to relaxation to the CIQCB bath (as shown in Figures 6 and 7 above), this primary $J_i = 12$ gateway channel is associated with V−V ET to an IR-dark vibrational level that we label arbitrarily as $(? ? ? ? ?)^?$.[32,49,50] The actual identity of this $(? ? ? ? ?)^?$ level remains uncertain, although it is likely to have $l > 0$ character

and be involved in local Coriolis and/or *l*-resonance perturbations. Using a rovibrational polyad/cluster model,[27] we have tentatively assigned it as $(0\ 3\ 0\ 10\ 1)^1/(1\ 0\ 2\ 4\ 1)^1$, with Π_u ($l = 1$) symmetry and mixed vibrational basis-state parentage.[29,30] We have also recognized less prominent secondary gateway channels,[49,50] such as the $(1\ 0\ 3\ 0\ 0)^0$ main and perturber rovibrational states with $J_i = 18$ and 17.[31,54] Also (as mentioned in Section III), an IR-dark $J_i = 16$ state is assigned tentatively to another unidentified IR-dark vibrational level with interim $(\#\ \#\ \#\ \#\ \#)^\#$ label.[49,50] Other aspects of such *J*-specific gateway channels, relevant to our master-equation model of collision-induced kinetics in the $4\nu_{CH}$ manifold of C_2H_2, are considered elsewhere.[49,50]

The time-resolved, LIF-detected IR−UV DR techniques that we use for state-specific investigations of collision-induced effects in C_2H_2 gas[24−32] are based on methodology established by Crim and co-workers.[18−23] They belong to a large family of experimental approaches that afford insight into an assortment of dynamical processes occurring primarily within rovibrational levels of the S_0 (linear, $\tilde{X}\ ^1\Sigma_g^+$) electronic ground state of C_2H_2. As part of this family, directly observed infrared absorption spectra have yielded an extensive vibrational-spectroscopic database[35−39,65,69−71] and have enabled a global fit of the vibrational energy pattern to available spectroscopic data up to $\sim$19 000 cm^{-1} in terms of the polyad/cluster model. Likewise, measurement of dispersed rovibronic LIF from the S_1 (transbent $\tilde{A}\ ^1A_u$) electronic state, entailing laser excitation of a single low-*J* $\tilde{A}-\tilde{X}$ transition (either under gas-phase conditions that allow collisional relaxation or collision-free in a molecular beam) combined with elegant numerical pattern-recognition methods, also provide an alternative direct spectroscopic view of vibrational states of C_2H_2 at high energies (typically 6 000−20 000 cm^{-1}).[41,71,72] A complementary spectroscopic technique, also relatively direct, is stimulated emission pumping (SEP),[17] which has been applied extensively to high-energy vibrational states of C_2H_2.[60d,73,74] Spectroscopic databases derived as above include many important homogeneous vibrational perturbations (e.g., anharmonic mixing and vibrational *l*-doubling) that can be characterized in the low-*J* limit. However, local *J*-dependent perturbations (e.g., rotational *l*-resonance and Coriolis coupling) tend to be treated on a case-by-case basis.[27,31,54,69,74]

As reported previously,[30,31] another relevant direct spectroscopic technique is that of Halonen and co-workers,[75,76] who have made dispersed rovibrational LIF measurements of C_2H_2 excited in the 12 700 cm^{-1} $4\nu_{CH}$ and 11 600 cm^{-1} $\nu_{CC} + 3\nu_{CH}$ regions, paralleling our IR−UV DR experiments.[24−32] Their observed odd-ΔJ collision-induced satellite features[76] are attributed to intermolecular vibrational step-down processes that scramble the ortho and para nuclear-spin modifications of C_2H_2, but without needing to break the strongly conserved *a*/*s* nuclear-spin symmetry. It is significant that there is no sign in these dispersed rovibrational LIF measurements[76] of unexpected CIQCB and/or odd-ΔJ ET phenomena that are observed in our IR−UV DR experiments detected by rovibronic LIF.[28−32] This is probably understandable in terms of the low sensitivity of rovibrational LIF relative to rovibronic LIF.

Our investigations[28−32] of the $4\nu_{CH}$ rovibrational manifold of C_2H_2 at $\sim$12 700 cm^{-1} by time-resolved, LIF-detected IR−UV DR spectroscopy are complemented by several other indirect spectroscopic techniques that entail assorted forms of molecular action, generally more complicated than simple absorption or emission of radiation. Such indirect spectroscopic techniques, addressing processes in the C_2H_2 $4\nu_{CH}$ rovibrational manifold, include optothermally detected molecular-beam laser-Stark spectroscopy[77] and pulsed two-step IR−UV excitation of dissociative H-atom action spectroscopy.[78] This variety of direct and indirect spectroscopic methods, which has been reviewed more thoroughly in our recent papers,[30−32] enables interesting local rovibrational perturbations to be viewed from several aspects and compared with our IR−UV DR results. However, a number of distinctive phenomena (e.g., CIQCB and/or odd-ΔJ ET effects) observed by our IR−UV DR technique are not found by these other experimental methods (including collision-induced dispersed rovibrational LIF[76]). We attribute such differences to the relatively high sensitivity and state-specificity that derives advantageously from the temporal sequence of IR PUMP, UV PROBE, and UV LIF detection that we employ.

Finally, we emphasize that our LIF-detected, time-resolved IR−UV DR approach, applied to C_2H_2, has enabled measurement and detailed characterization of an unexpected CIQCB effect.[29,30−32,49,50,53] This is facilitated by higher-than-usual detection sensitivity and the highly symmetric structure and spectroscopic amenability of the C_2H_2 molecule. Such observations are particular to our IR−UV DR experimental approach, relying on the UV PROBE to project UV-bright states out of a highly perturbed rovibrational manifold with low Franck−Condon factors. Similar effects may yet be discovered in larger molecules with less simple structure. In the meantime, the CIQCB phenomenon should probably be regarded as a significant dynamical possibility that might underlie physical and chemical processes in other polyatomic molecules, rather than a mere mechanistic curiosity confined to C_2H_2 alone.

Acknowledgment. Financial support from the Australian Research Council (ARC) is gratefully acknowledged, including the award of an ARC Postdoctoral Fellowship to one of us (A.P.M.).

References and Notes

(1) Moore, C. B. *Adv. Chem. Phys.* **1973**, *23*, 41.
(2) Weitz, E.; Flynn, G. *Annu. Rev. Phys. Chem.* **1974**, *25*, 275.
(3) Yardley, J. T. *Introduction to Molecular Energy Transfer*; Academic Press: New York, 1980.
(4) Orr, B. J.; Smith, I. W. M. *J. Phys. Chem.* **1987**, *91*, 6106.
(5) Orr, B. J. *Chem. Phys.* **1995**, *190*, 261.
(6) Orr, B. J. In *Advances in Chemical Kinetics and Dynamics − Vibrational Energy Transfer Involving Large and Small Molecules*; Barker, J. R., Ed.; JAI Press: Greenwich, CT, 1995; Vol. 2A, p 21.
(7) Flynn, G. W.; Parmenter, C. S.; Wodtke, A. M. *J. Phys. Chem.* **1996**, *100*, 12817.
(8) (a) Quack, M.; Troe, J. *Int. Rev. Phys. Chem.* **1981**, *1*, 97. (b) Hippler, H.; Troe, J. In *Advances in Gas-Phase Photochemistry and Kinetics: Bimolecular Collisions*; Ashfold, M. N. R., Baggott, J. E., Eds; The Royal Society of Chemistry: London, 1989; p 209.
(9) Oref, I.; Tardy, D. C. *Chem. Rev.* **1990**, *77*, 1407.
(10) (a) Gilbert, R. G.; Smith, S. C. *Theory of Unimolecular and Recombination Reactions*; Blackwell Scientific: Oxford, U.K., 1990. (b) Gilbert, R. G. *Int. Rev. Phys. Chem.* **1991**, *10*, 319.
(11) Weston, R. E.; Flynn, G. W. *Annu. Rev. Phys. Chem.* **1992**, *43*, 559.
(12) (a) Troe, J. *Ber. Bunsen-Ges. Phys. Chem.* **1994**, *98*, 102. (b) Troe, J. *Faraday Discuss.* **1995**, *102*, 485.
(13) Baer, T.; Hase, W. L. *Unimolecular Reaction Dynamics. Theory and Experiments*; Oxford University Press: New York, 1996.
(14) Barker, J. R.; Yoder, L. M.; King, K. D. *J. Phys. Chem. A* **2001**, *105*, 796.
(15) Quack, M. *Annu. Rev. Phys. Chem.* **1990**, *41*, 839.
(16) (a) Lehmann, K. K.; Scoles, G.; Pate, B. H. *Annu. Rev. Phys. Chem.* **1994**, *45*, 241. (b) Keske, J.; McWhorter, D. A.; Pate, B. H. *Int. Rev. Phys. Chem.* **2000**, *19*, 363. (c) Keske, J. C.; Pate, B. H. *Annu. Rev. Phys. Chem.* **2000**, *51*, 323.
(17) (a) Nesbitt, D. J.; Field, R. W. *J. Phys. Chem.* **1996**, *100*, 12735. (b) Silva, M.; Jongma, R.; Field, R. W.; Wodtke, A. M. *Annu. Rev. Phys. Chem.* **2001**, *52*, 811.
(18) Carrasquillo M. E.; Utz, A. L.; Crim, F. F. *J. Chem. Phys.* **1988**, *88*, 5976.

(19) Utz, A. L.; Tobiason, J. D.; Carrasquillo M. E.; Fritz, M. D.; Crim, F. F. *J. Chem. Phys.* **1992**, *97*, 389.
(20) Tobiason, J. D.; Utz, A. L.; Crim, F. F. *J. Chem. Phys.* **1992**, *97*, 7437.
(21) Tobiason, J. D.; Utz, A. L.; Crim, F. F. *J. Chem. Phys.* **1994**, *101*, 1108.
(22) Tobiason, J. D.; Fritz, M. D.; Crim, F. F. *J. Chem. Phys.* **1994**, *101*, 9642.
(23) Utz, A. L.; Carrasquillo M., E.; Tobiason, J. D.; Crim, F. F. *Chem. Phys.* **1995**, *190*, 311.
(24) Milce, A. P.; Barth, H.-D.; Orr, B. J. *J. Chem. Phys.* **1994**, *100*, 2398.
(25) Milce, A. P.; Orr, B. J. *J. Chem. Phys.* **1996**, *104*, 6423.
(26) Milce, A. P.; Orr, B. J. *J. Chem. Phys.* **1997**, *106*, 3592.
(27) Milce, A. P.; Orr, B. J. *J. Chem. Phys.* **2000**, *112*, 9319.
(28) Payne, M. A.; Milce, A. P.; Frost, M. J.; Orr, B. J. *Chem. Phys. Lett.* **1997**, *265*, 244.
(29) Payne, M. A.; Milce, A. P.; Frost, M. J.; Orr, B. J. *Chem. Phys. Lett.* **2000**, *324*, 48.
(30) Payne, M. A.; Milce, A. P.; Frost, M. J.; Orr, B. J. *J. Phys. Chem. A* **2003**, *107*, 10759.
(31) Payne, M. A.; Milce, A. P.; Frost, M. J.; Orr, B. J. *J. Phys. Chem. B* **2005**, *109*, 8332.
(32) Payne, M. A.; Milce, A. P.; Frost, M. J.; Orr, B. J. *Z. Phys. Chem.* **2005**, *219*, 601.
(33) Abel, B.; Lange, N.; Reiche, F.; Troe, J. *J. Chem. Phys.* **1999**, *110*, 1389.
(34) Abel, B.; Lange, N.; Reiche, F.; Troe, J. *J. Chem. Phys.* **1999**, *110*, 1404.
(35) Herman, M.; Liévin, J.; Vander Auwera, J.; Campargue, A. *Adv. Chem. Phys.* **1999**, *108*, 1.
(36) Herman, M.; Campargue, A.; El Idrissi, M. I.; Vander Auwera, J. *J. Phys. Chem. Ref. Data* **2003**, *32*, 921
(37) Jacquemart, D.; Mandin, J.-Y.; Dana, V.; Claveau, C.; Vander Auwera, J.; Herman, M.; Rothman, L. S.; Regalia-Jarlot, L.; Barbe, A. *J. Quant. Spectrosc. Radiat. Transfer* **2003**, *82*, 363.
(38) Perevalov, V. I.; Lyulin, O. M.; Jacquemart, D.; Claveau, C.; Teffo, J.-L.; Dana, V.; Mandin, J.-Y.; Valentin, A. *J. Mol. Spectrosc.* **2003**, *218*, 180.
(39) Rothman, L. S.; Jacquemart, D.; Barbe, A.; Chris Benner, D.; Birk, M.; Brown, L. R.; Carleer, M. R.; Chackerian, C., Jr.; Chance, K.; Coudert, L. H.; Dana, V.; Devi, V. M.; Flaud, J.-M.; Gamache, R. R.; Goldman, A.; Hartmann, J.-M.; Jucks, K. W.; Maki, A. G.; Mandin, J.-Y.; Massie, S. T.; Orphal, J.; Perrin, A.; Rinsland, C. P.; Smith, M. A. H.; Tennyson, J.; Tolchenov, R. N.; Toth, R. A.; Vander Auwera, J.; Varanasi, P.; Wagner, G. *J. Quant. Spectrosc. Radiat. Transfer* **2005**, *96*, 139.
(40) Srivastava, H. K.; Conjusteau, A.; Mabuchi, H.; Lehmann, K. K.; Scoles, G.; Silva, M. L.; Field, R. W. *J. Chem. Phys.* **2000**, *113*, 7376.
(41) Jacobson, M. P.; Field, R. W. *J. Phys. Chem. A* **2000**, *104*, 3073.
(42) Schork, R.; Köppel, H. *J. Chem. Phys.* **2001**, *115*, 7907.
(43) (a) Zou, S.; Bowman, J. M. *J. Chem. Phys.* **2002**, *116*, 6667. (b) Zou, S.; Bowman, J. M. *J. Chem. Phys.* **2002**, *117*, 5507. (c) Zou, S.; Bowman, J. M. *Chem. Phys. Lett.* **2002**, *368*, 421. (d) Zou, S.; Bowman, J. M.; Brown, A. *J. Chem. Phys.* **2003**, *118*, 10012. (e) Xu, D.; Guo, H.; Zou, S.; Bowman, J. M. *Chem. Phys. Lett.* **2003**, *377*, 582.
(44) Loh, Z.-H.; Field, R. W. *J. Chem. Phys.* **2003**, *118*, 4037.
(45) Yang, S.; Tyng, V.; Kellman, M. E. *J. Phys. Chem. A* **2003**, *107*, 8345.
(46) Bittner, M.; Köppel, H. *Phys. Chem. Chem. Phys* **2003**, *5*, 4604.
(47) Kozin, I. N.; Law, M. M.; Tennyson, J. M.; Hutson, J. M. *J. Chem. Phys.* **2005**, *122*, 064309.
(48) Herregodts, F.; Kerrinckx, E.; Huet, T. R.; Vander Auwera, J. *Mol. Phys.* **2003**, *101*, 3427.
(49) Payne, M. A. Ph.D. Thesis, Macquarie University, Sydney, Australia, 1999.
(50) Payne, M. A.; Milce, A. P.; Frost, M. J.; Orr, B. J. Unpublished results.
(51) Brown, J. M.; Hougen, J. T.; Huber, K.-P.; Johns, J. W. C.; Kopp, I.; Lefebvre-Brion, H.; Merer, A. J.; Ramsay, D. A.; Rostas, J.; Zare, R. N. *J. Mol. Spectrosc.* **1975**, *55*, 500.
(52) Utz, A. L.; Tobiason, J. D.; Carrasquillo, M. E.; Sanders, L. J.; Crim, F. F. *J. Chem. Phys.* **1993**, *98*, 2742.
(53) Baxter, G. W.; Payne, M. A.; Austin, B. D. W.; Halloway, C. A.; Haub, J. G.; He, Y.; Milce, A. P.; Nibler, J. W.; Orr, B. J. *Appl. Phys. B* **2000**, *71*, 651.
(54) Hurtmans, D.; Kassi, S.; Depiesse, C.; Herman, M. *Mol. Phys.* **2002**, *100*, 3507.
(55) Foo, P. D.; Innes, K. K. *Chem. Phys. Lett.* **1973**, *22*, 439.
(56) (a) Zhang, J.; Riehn, C. W.; Dulligan, M.; Wittig, C. *J. Chem. Phys.*, **1995**, *103*, 6815. (b) Arusi-Parpar, T.; Schmid, R. P.; Ganot, Y.; Bar, I.; Rosenwaks, S. *Chem. Phys. Lett.* **1998**, *287*, 347.
(57) Liu, L.; Muckerman, J. T. *J. Chem. Phys.* **1999**, *110*, 2446.
(58) O'Brien, J. P.; Jacobson, M. P.; Sokol, J. J.; Coy, S. L.; Field, R. W. *J. Chem. Phys.* **1998**, *108*, 7100.
(59) Watson, J. K. G.; Herman, M.; Van Craen, J. C.; Colin, R. *J. Mol. Spectrosc.* **1982**, *95*, 101.
(60) (a) Fujii, M.; Haijima, A.; Ito, M. *Chem. Phys. Lett.* **1988**, *150*, 380. (b) Haijima, A.; Fujii, M.; Ito, M. *J. Chem. Phys.* **1990**, *92*, 959. (c) Drabbels, M.; Heinze, J.; Meerts, W. L. *J. Chem. Phys.* **1994**, *100*, 165. (d) Drucker, S.; O'Brien, J. P.; Patel, P.; Field, R. W. *J. Chem. Phys.* **1997**, *106*, 3423. (e) Suzuki, T.; Shi, Y.; Kohguchi, H. *J. Chem. Phys.* **1997**, *106*, 5292. (f) Suzuki, T.; Hashimoto, N. *J. Chem. Phys.* **1999**, *110*, 2042. (g) Ahmed, M.; Peterka, T. S.; Suits, A. G. *J. Chem. Phys.* **1999**, *110*, 4248.
(61) Mishra, A. P.; Thom, R. L.; Field, R. W. *J. Mol. Spectrosc.* **2004**, *228*, 565.
(62) Makarov, V. I.; Khmelinskii, I. V. *Chem. Phys. Lett.* **2005**, *402*, 352.
(63) (a) Sherrill, C. D.; Vacek, G.; Yamaguchi, Y.; Schaefer, H. F.; Stanton, J. F.; Gauss, J. *J. Chem. Phys.* **1996**, *104*, 8507. (b) Cui, Q.; Morokuma, K.; Stanton, J. F. *Chem. Phys. Lett.* **1996**, *263*, 46. (c) Cui, Q.; Morokuma, K. *Chem. Phys. Lett.* **1997**, *272*, 319. (d) Le, H. T.; Flock, M.; Nguyen, M. T. *J. Chem. Phys.* **2000**, *112*, 7008.
(64) Mordaunt, D. H.; Ashfold, M. N. R. *J. Chem. Phys.* **1994**, *101*, 2630.
(65) (a) Abboutti Temsamani, M.; Herman, M. *J. Chem. Phys.* **1995**, *102*, 6371. (b) El Idrissi, M. I.; Liévin, J.; Campargue, A.; Herman, M. *J. Chem. Phys.* **1999**, *110*, 2074.
(66) Nizamov, B.; Yang, X.; Dagdigian, P. J.; Alexander, M. H. *J. Phys. Chem. A* **2002**, *106*, 8345.
(67) Bernshtein, V.; Oref, I. *J. Phys. Chem. B* **2005**, *109*, 8310.
(68) Koifman, I.; Dashevskaya, E. I.; Nikitin, E. E.; Troe, J. *J. Phys. Chem.* **1995**, *99*, 15348.
(69) Abboutti Temsamani, M.; Herman, M. *J. Chem. Phys.* **1996**, *105*, 1355.
(70) Campargue, A.; Abboutti Temsamani, M.; Herman, M. *Mol. Phys.* **1997**, *90*, 793.
(71) Abboutti Temsamani, M.; Herman, M.; Solina, S. A. B.; O'Brien, J. P.; Field, R. W. *J. Chem. Phys.* **1996**, *105*, 11357.
(72) (a) Solina, S. A. B.; O'Brien, J. P.; Field, R. W.; Polik, W. F. *Ber. Bunsen-Ges. Phys. Chem.* **1995**, *99*, 555. (b) Solina, S. A. B.; O'Brien, J. P.; Field, R. W.; Polik, W. F. *J. Phys. Chem.* **1996**, *100*, 7797. (c) Jacobson, M. P.; O'Brien, J. P.; Silbey, R. J.; Field, R. W. *J. Chem. Phys.* **1998**, *109*, 121. (d) Jacobson, M. P.; O'Brien, J. P.; Field, R. W. *J. Chem. Phys.* **1998**, *109*, 3831. (e) Hoshina, K.; Iwasaki, A.; Yamanouchi, K.; Jacobson, M. P.; Field, R. W. *J. Chem. Phys.* **2001**, *114*, 7424. (f) Silva, M. L.; Jacobson, M. P.; Duan, Z.; Field, R. W. *J. Chem. Phys.* **2002**, *116*, 7939.
(73) Jonas, D. M.; Solina, S. A. B.; Rajaram, B.; Silbey, R. J.; Field, R. W.; Yamanouchi, K.; Tsuchiya, S. *J. Chem. Phys.* **1993**, *99*, 7350.
(74) Moss, D. B.; Duan, Z.; Jacobson, M. P.; O'Brien, J. P.; Field, R. W. *J. Mol. Spectrosc.* **2000**, *199*, 265.
(75) (a) Jungner, P.; Halonen, L. *J. Chem. Phys.* **1997**, *107*, 1680. (b) Saarinen, M.; Permogorov, D.; Halonen, L. *J. Chem. Phys.* **1999**, *110*, 1424.
(76) Metsälä, M.; Yang, S.; Vaittinen, O.; Halonen, L. *J. Chem. Phys.* **2002**, *117*, 8686.
(77) (a) Barnes, J. A.; Gough, T. E.; Stoer, M. *Chem. Phys. Lett.* **1995**, *237*, 437. (b) Barnes, J. A.; Gough, T. E.; Stoer, M. *Rev. Sci. Instrum.* **1999**, *70*, 3515. (c) Barnes, J. A.; Gough, T. E.; Stoer, M. *J. Chem. Phys.* **2001**, *114*, 4490.
(78) Sheng, X.; Ganot, Y.; Rosenwaks, S.; Bar, I. *J. Chem. Phys.* **2002**, *117*, 6511.